UNIVERSITAT POLITÈCNICA DE CATALUNYA
BARCELONATECH
Escola d'Enginyeria de Telecomunicació
i Aeroespacial de Castelldefels

# TREBALL DE FI DE GRAU

**TFG TITLE: Design of a low-latency transoceanic shortwave radio link for High Frequency Trading applications**

**DEGREE: Bachelor's Degree in Telecommunications Systems**

**AUTHOR: Maria Vallès Muñoz**

**ADVISOR: Eduard Úbeda Farré**

**DATE: October 22, 2019**

**Title :** Design of a low-latency transoceanic shortwave radio link for High Frequency Trading applications

**Author:** Maria Vallès Muñoz

**Advisor:** Eduard Úbeda Farré

**Date:** October 22, 2019

**Overview**

The main objective of this final Bachelor's degree project is to design and study the reliability of a transoceanic shortwave radio link that connects London and New York. Two of the most important stock exchanges of the world are located in these two cities and the connection between them is currently done through submarine optical fibers.
In the last few years, with the automation of the stock market activity (a trend that is also known as High Frequency Trading), several companies have begun to look for alternatives to optical fiber to reduce the latency of the link use this advantage to be more competitive. However, before designing the radio link, the behaviour of the ionosphere has been studied to correctly understand how ionospheric propagation works and what factors can compromise the communication.
The radio link design is based on the choice of different aspects such as the location of the stations, the type of antenna, the protocol or the propagation mode, among others. This selection has been made prioritizing the reliability of the link over other aspects such as the capacity or the bandwidth.
Once these aspects have been decided, the communication has been studied using an ionospheric propagation prediction software called VOACAP. This software gives us very relevant information about the reliability or the power received. This will allow us to model this propagation by relating the behaviour of the different frequency bands with the variations suffered by the ionosphere during the different months of the year and the different hours of the day.
On the other hand, this study demonstrates how the designed radio link substantially reduces the latency of the fiber optic with a high reliability that can allow its use regularly.

**Títol:** Disseny d'un radioenllaç transoceànic d'ona curta de baixa latència per a aplicacions de High Frequency Trading
**Autor:** Maria Vallès Muñoz

**Director:** Eduard Úbeda Farré

**Data:** 22 d'octubre de 2019

**Resum**

L'objectiu principal d'aquest treball de fi de grau és dissenyar i estudiar la fiabilitat d'un radioenllaç transoceànic d'ona curta que connecti Londres i Nova York. A aquestes dues ciutats es troben dues de les borses més importants a nivell mundial, i actualment la connexió entre elles es realitza amb fibra òptica submarina.
Els darrers anys, amb l'automatització de l'activitat borsària (tendència que també es coneix amb el nom de *High Frequency Trading*), diverses empreses han començat a buscar alternatives a la fibra òptica per tal de reduir la latència de l'enllaç i aprofitar aquest avantatge per ser més competitives. Abans de dissenyar el radioenllaç, però, s'ha estudiat a fons el comportament de la ionosfera per entendre correctament com funciona la propagació ionosfèrica i quins són els factors que poden comprometre el correcte funcionament de l'enllaç.
El disseny del radioenllaç està basat en l'elecció, entre d'altres, de la ubicació de les dues estacions, el tipus d'antena, el protocol, la modulació, la potència transmesa o el mode de propagació. Aquesta tria s'ha fet sempre prioritzant la fiabilitat de l'enllaç per davant d'altres aspectes com poden ser la capacitat o l'amplada de banda.
Un cop decidits aquests aspectes, s'ha estudiat la comunicació utilitzant un software de predicció de propagació ionosfèrica anomenat VOACAP. Aquest software ens dóna informació molt rellevant sobre la fiabilitat o la potència rebuda. Això ens permetrà modelar aquesta propagació relacionant el comportament de les diferents bandes freqüencials amb les variacions que pateix la ionosfera durant els diferents mesos de l'any i les diferents hores del dia.
D'altra banda, aquest estudi demostra com el radioenllaç dissenyat redueix substancialment la latència de la connexió per fibra òptica, oferint una fiabilitat elevada que podrà permetre el seu ús de forma regular.

Als meus pares, que m'han inculcat els valors del treball i de l'esforç
i sempre m'han encoratjat a superar-me.
A la Leire, que m'ha recolzat en els moments difícils
i sempre m'ha animat a seguir endavant.
Al meu germà, a la meva família i a tots els que heu fet possible
que aquest TFG vegi la llum.

# CONTENTS


**ACRONYMS** . . . . . 1

**Introduction** . . . . . 3

**CHAPTER 1. Introduction to High frequency radio propagation** . . 5

**1.1. The ionosphere** . . . . . 5

1.1.1. Layers of the ionosphere . . . . . 6

1.1.2. Ionosphere variations . . . . . 9

**CHAPTER 2. High Frequency Communications** . . . . . 13

**2.1. Amateur propagation bands** . . . . . 13

2.1.1. 80 meter band . . . . . 13

2.1.2. 60 meter band . . . . . 13

2.1.3. 40 meter band . . . . . 14

2.1.4. 30 meter band . . . . . 14

2.1.5. 20 meter band . . . . . 14

2.1.6. 17 meter band . . . . . 14

2.1.7. 15 meter band . . . . . 15

2.1.8. 12 meter band . . . . . 15

2.1.9. 10 meter band . . . . . 15

**2.2. The Usable Frequency Range** . . . . . 15

2.2.1. Maximum Usable Frequency (MUF) . . . . . 15

2.2.2. Lowest Usable Frequency (LUF) . . . . . 16

2.2.3. Frequency of Optimum Transmission (FOT) . . . . . 16

2.2.4. Ionospheric sounders . . . . . 16

**2.3. Hop Length** . . . . . 17

**2.4. Propagation modes** . . . . . 18

**2.5. Noise** . . . . . 19

2.5.1. Interference . . . . . 20

2.5.2. Atmospheric noise . . . . . 20

2.5.3. Man-made noise . . . . . 21

2.5.4. Galactic noise . . . . . 21

**CHAPTER 3. High frequency trading** . . . . . **23**

**3.1. Introduction** . . . . . **23**

**3.2. The importance of HF Propagation in HFT** . . . . . **25**

**CHAPTER 4. Link** . . . . . **27**

**4.1. Basic description** . . . . . **27**

**4.2. Sites location** . . . . . **28**

4.2.1. US site . . . . . 28

4.2.2. UK site . . . . . 29

**4.3. Antennas** . . . . . **30**

**4.4. Protocol and modulation** . . . . . **33**

**4.5. Transmitted power** . . . . . **34**

**4.6. Number of hops** . . . . . **34**

**CHAPTER 5. VOACAP software** . . . . . **35**

**5.1. Software inputs** . . . . . **35**

5.1.1. TX and RX location . . . . . 35

5.1.2. Day and hour . . . . . 36

5.1.3. Transmitting Mode menu . . . . . 36

5.1.4. Transmitting Power menu . . . . . 36

5.1.5. Antennas button . . . . . 37

5.1.6. Settings button . . . . . 37

**5.2. Software outputs** . . . . . **39**

5.2.1. Circuit Reliability chart . . . . . 39

5.2.2. 24-hour propagation prediction wheel . . . . . 40

5.2.3. SDBW chart . . . . . 40

**CHAPTER 6. Simulation results** . . . . . **43**

**6.1. Winter Season** . . . . . **43**

**6.2. Spring Season** . . . . . **43**

**6.3. Summer season** . . . . . **44**

**6.4. Autumn season** . . . . . **44**

**6.5. Summary of the simulation results** . . . . . **45**

**CHAPTER 7. Latency comparison between HF and optical fiber links** . . . . . **55**

**7.1. HF link** . . . . . **55**

**7.2. Optical fiber link** . . . . . **57**

7.2.1. Apollo North cable . . . . . 58

7.2.2. Yellow/AC-2 cable . . . . . 59

**Conclusions** . . . . . **61**

**Bibliography** . . . . . **63**

# LIST OF FIGURES


1.1 Relationship between the regions of the atmosphere and the ionosphere . . . . 5
1.2 Ionospheric layers and their electron densities as a function of height (in km) above the Earth's surface . . . . 6
1.3 Ionospheric layers as a function of height above the Earth's surface (Source: [5]) 7
1.4 Sporadic E-layer propagation (Source: [6]) . . . . 9
1.5 A gigantic sunspot of almost 130000 kilometres across on the Sun's surface captured in 2014 by the National Aeronautics and Space Administration (NASA) (Source: [12]) . . . . 10
1.6 The relationship between sunspots and critical frequencies of E, F1 and F2 layers in Canberra, Australia, from 1988 to 2005 (Source: [6]) . . . . 11

2.1 ITU regions (Source: [13]) . . . . 13
2.2 Ionogram (Source: [5]) . . . . 17
2.3 Hop lengths for two different situations (Source: [6]) . . . . 17
2.4 The relationship between the takeoff angle (in degrees) and the hop length (in km) (Source: [3]) . . . . 18
2.5 Simple propagation modes (Source: [6]) . . . . 18
2.6 Complex propagation modes (Source: [6]) . . . . 19
2.7 $F_a$ depending on the frequency (Source: [17]) . . . . 20
2.8 Median values of man-made noise power (Source: [17]) . . . . 22

3.1 HFT as a share of United States (US) equities daily volume (Source: [20]) . . . . 23
3.2 Comparison between trades and quotes from 2006 to 2012 (Source: [22]) . . . . 24
3.3 Camouflaged antenna in Wesley Hills, New York (Source: [24]) . . . . 26

4.1 Basic structure of our system . . . . 27
4.2 Google Maps screenshots of the location of the US site . . . . 28
4.3 Google Maps screenshot of the distance between the site and New York . . . . 29
4.4 Google Maps screenshots of the location of the UK site . . . . 29
4.5 Google Maps screenshot of the distance between the site and London . . . . 29
4.6 10-30LP8 and 7&10-30LP8 antennas . . . . 30
4.7 Log-periodic dipole array structure (Source: [31]) . . . . 31
4.8 Main connection methods for log-periodic arrays . . . . 32
4.9 Comparison between 2FSK and 2GFSK spectra (Source: [37]) . . . . 33

5.1 VOACAP's main map (Source: [40]) . . . . 35
5.2 SSN (Source: [42]) . . . . 38
5.3 Reliability chart (Source: [40]) . . . . 40
5.4 24-hour propagation prediction wheel (Source: [40]) . . . . 41
5.5 SDBW chart (Source: [40]) . . . . 41

6.1 VOACAP reliability charts for December, January and February . . . . 46
6.2 VOACAP SDBW charts for December, January and February . . . . 47

6.3 VOACAP reliability charts for March and April and Propagation Prediction Wheel for May . . . . . 48
6.4 VOACAP SDBW charts for March, April and May . . . . . 49
6.5 VOACAP reliability charts for June, July and August . . . . . 50
6.6 VOACAP reliability charts for September, October and November . . . . . 51
6.7 VOACAP SDBW charts for September with TX powers of 200 W and 1500 W . 52

7.1 Geometric representation of a HF path between points A and B (Source: [3]) . . 55
7.2 Schematic view of the path . . . . . 56
7.3 VOACAP screenshot of the path's midpoint (Source: [40]) . . . . . 56
7.4 Latency contributions in an optical fiber system (Source: [43]) . . . . . 57
7.5 Submarine Cable Map website screenshot (Source: [44]) . . . . . 58
7.6 Apollo submarine cables (Source: [47]) . . . . . 58
7.7 Yellow/AC-2 submarine cable (Source: [48]) . . . . . 59

# LIST OF TABLES

1.1 Height and electron density of ionospheric layers (Sources: [4] [7]) . . . . . 6

2.1 Different frequency ranges for each ITU region (Source: [16]) . . . . . 14
2.2 Environmental categories defined by the ITU (Sources: [3]) . . . . . 21

4.1 Specification comparison between 10-30LP8 and 7&10-30LP8 antennas (Source: [29] [30]) . . . . . 31
4.2 Correlation between VSWR and the percentage of returned power (Source: [33]) 32
4.3 Radio amateur protocols and its modulations (Sources: [34] [35] [36]) . . . . . 33

5.1 Antennas chosen for each band . . . . . 37
5.2 Input parameters for the simulations . . . . . 39
5.3 S-meter scale (Source: [41]) . . . . . 40

6.1 Selected amateur bands for different months . . . . . 53

# ACRONYMS

**AM** Amplitude Modulation

**CW** Continuous Wave

**foE** Critical Frequency of the E-layer

**foF1** Critical Frequency of the F1-layer

**foF2** Critical Frequency of the F2-layer

**FOT** Frequency of Optimum Transmission

**FSK** Frequency Shift Keying

**GFSK** Gaussian Frequency Shift Keying

**HF** High Frequency

**HFT** High Frequency Trading

**ISI** Intersymbol Interference

**ITU** International Telecommunication Union

**LUF** Lowest Usable Frequency

**MUF** Maximum Usable Frequency

**NASA** National Aeronautics and Space

**OWF** Optimum Working Frequency

**RF** Radio frequency

**RX** Receiver

**SDBW** Signal Power in dBW

**SEC** Securities and Exchange Comission

**SILSO** Sunspot Index and Long-term Solar Observations

**SNR** Signal-to-Noise Ratio

**SSB** Single Side Band

**SSN** Smoothed Sunspot Number

**TOA** Takeoff Angle

**TX** Transmitter

**UTC** Coordinated Universal Time

**VOACAP** Voice Of America Coverage Analysis Program

**VSWR** Voltage Standing Wave Ratio

**WARC** World Administrative Radio Conference

**WSPR** Weak Signal Propagation Reporter

# INTRODUCTION

Although high frequency (HF) propagation plays a key role in modern wireless communications, first experiments on electromagnetic waves started at the end of the nineteenth century. In 1888, Heinrich Hertz proved that waves propagate at speed of light. This theory, however, had been formulated by Maxwell a couple of decades before. About ten years later, Guglielmo Marconi succeeded in sending the first transoceanic transmission between England and Canada. Nevertheless, Marconi thought that the radio wave had followed the curvature of the Earth, and he was wrong. What really happened was that the radio wave was reflected by the ionosphere.

Since then, many people began to investigate and experiment with radio waves. These people are considered the first radio amateurs and made simple communications in morse code. Nowadays, although there are still many radio amateurs operating around the world, a downward trend has occurred, probably due to the emergence of new technologies that improve communications performance.

Even so, HF propagation still has some advantages over other types of communication such as fiber optics. On the one side, a microwave link can be installed in a very short time and with a reduced economic investment compared to the optical fiber. Moreover, we add that the communication of interest is transoceanic, deployment and maintenance costs increase. On the other side, a microwave link has a lower latency than a optical fiber one, as waves propagate faster through the air.

That is why in recent years, many enterprises, especially in the stock market sector, have started to experiment with shortwave radio to transmit trading information. For example, the company McKay Brothers has recently built a microwave link between Chicago and New York [1]. It is important to emphasise that, because of the automation of stock market activity, a few milliseconds can make a difference. This type of trading is also known as High Frequency Trading (HFT).

Despite the advantages that HF propagation offers, long-distance microwave links depend on the ionosphere, a very variable layer of the atmosphere. Its behaviour changes every hour, month, season or year, so it is very difficult to predict.

For all the above-mentioned reasons, it has been found interesting to study the behaviour of the ionosphere, as well as the influence that its variations may have on communications. Hence, this final Bachelor's degree project will focus on the design and study of reliability of a microwave link that connects London and New York, where two of the most important stock exchanges of the world are located.

The design will be based on the choice of different aspects related to the transmission. Among these, there are some that can be highlighted, such as the location of the stations, the type of antenna, the protocol, the modulation, the transmitting power or the propagation mode.

On the other hand, the study of the reliability of the link will be done with a software called VOACAP. This program allows users to simulate microwave communications between two points of the Earth and gives very valuable information about reliability, received power or propagation modes.

In this way, this study will try to demonstrate that it is possible to establish a microwave link

between these two cities with a lower latency than the current fiber optic link. The main requirement for this to happen is to achieve a high reliability.

After this introduction, the objectives of this project are presented in a summarized way.

- Study the behaviour of the ionosphere throughout a year
- Understand the main characteristics and particularities of the HF propagation
- Introduce ourselves to High Frequency Trading and understand the role that HF propagation may play in this field
- Design a transoceanic shortwave radio link between London and New York
- Study the reliability of the designed link using VOACAP software
- Estimate the latency of the designed link and compare it with the latency of the current fiber optic link
- Conclude whether it is feasible to establish this link

# CHAPTER 1. INTRODUCTION TO HIGH FREQUENCY RADIO PROPAGATION

Radio frequency (RF) transmission between 3 and 30 MHz is called high frequency or shortwave by the International Telecommunication Union (ITU) convention. Therefore, wavelengths are around tens of meters and can be also called as decametric waves [2].

HF waves are characterized by a ground-wave and a sky-wave component. The first one follows the Earth's surface and can provide successful communications over up to 1000 km. On the other hand, sky-wave transmission is based on ionospheric refraction and is used for long circuits over up to 12800 km [3].

Taking into account the defined objectives, this chapter will focus on explaining the behaviour of HF radio waves and their interaction with the ionosphere.

## 1.1. The ionosphere

The ionosphere is a region of the atmosphere extending from a height of 50 km to roughly 500 km. Thus, this region comprises the entire thermosphere layer and the upper part of the mesosphere layer. Even so, some ionisation irregularities that occur at the top of the ionosphere can extend the upper limit of the ionosphere many more kilometres [4]. Consequently, the ionosphere can also occupy the lowest part of the exosphere.

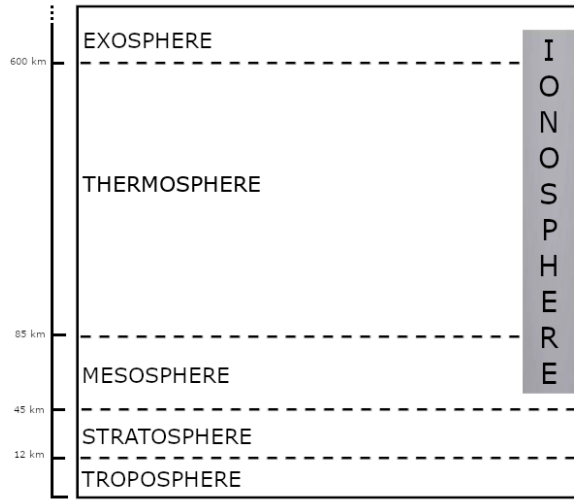


Figure 1.1: Relationship between the regions of the atmosphere and the ionosphere

Its name is due to the ionisation caused by solar radiation in its molecules. Ionisation is the phenomenon in which, through energy exchanges, principally oxygen and nitrogen gas molecules present in the atmosphere dissociate into atoms that can release electrons, resulting in free electrons with negative charge and ions with positive charge [5]. These free electrons cause HF radio waves to be reflected back to Earth. The greater the density of electrons, the higher the frequencies that can be reflected [6].

Principally, the main source of ionisation in the ionosphere is radiation from the Sun. However, not all solar rays are ionising: only ultra-violet and X-rays portions of the spectrum are considered ionising [4]. On the other hand, there are other sources of ionisation such as cosmic rays, which are generated by stars and other celestial events like supernova explosions, but their intensity is about 100 times lower than solar one [5].

### 1.1.1. Layers of the ionosphere

Obviously, the ionisation level of the ionosphere is greater during the day because both solar and cosmic rays affect the ionosphere. At night, without solar rays, only star cosmic rays ionise the ionosphere, but not as strong as the Sun does. For this reason, different layers are considered depending on whether it is day or night (see Figure 1.2).

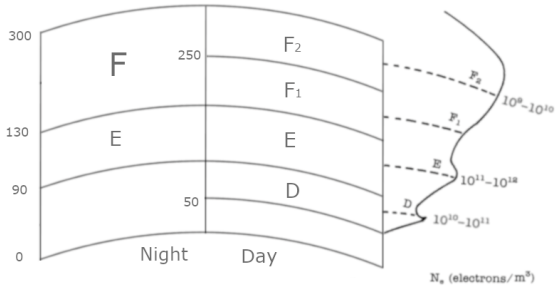


Figure 1.2: Ionospheric layers and their electron densities as a function of height (in km) above the Earth's surface

The main difference between layers is their electron density, which increases as the height rises. The height above the Earth's surface and the electron density of every ionospheric layer and is specified in Table 1.1.

| Ionospheric layer | Height [km] | Electron density [e/mˆ3] |
|---|---|---|
| D-layer | 50-90 | ∼10ˆ9 |
| E-layer | 90-130 | ∼10ˆ11 |
| F-layer | 130-300 | ∼10ˆ12 |

Table 1.1: Height and electron density of ionospheric layers (Sources: [4] [7])

The maximum electron density is a very important fact regarding ionospheric propagation since it defines the maximum frequency that each layer can reflect back to the Earth's surface. This frequency is also called critical frequency and it can be calculated using the following equation [7]

$$f_{max} = 8.98\sqrt{N_e} \tag{1.1}$$

where:

$f_{max}$ = critical frequency
$N_e$ = electron density

Although it can be calculated this way, it is usually obtained empirically using ionospheric sounders. This is going to be explained in 2.2.4.. The appropriate notation to define the critical frequencies of E, F1 and F2 layers is foE, foF1 and foF2.

Even though we talk about reflection, we should really talk about refraction. As we know, the ionisation density of the ionosphere is not homogeneous. In Figure 1.3 we consider a region of the ionosphere where every layer has a different value of ionisation density $Ni$ and therefore a different refractive index so that $0 < N_1 < N_2 < ... < N_k$.

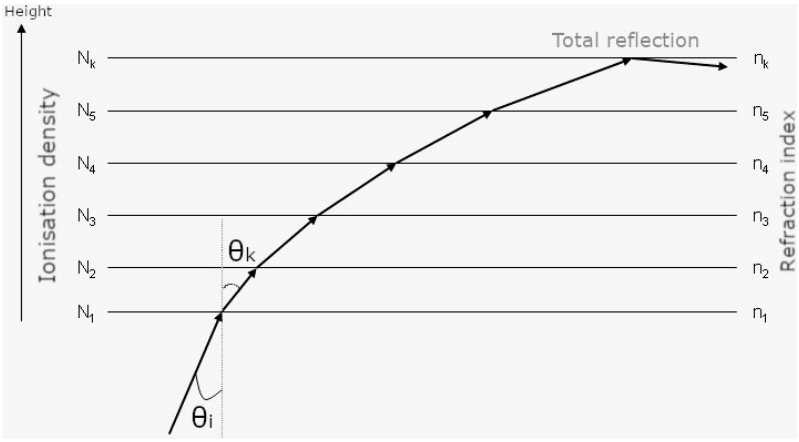


Figure 1.3: Ionospheric layers as a function of height above the Earth's surface (Source: [5])

Radio waves are refracted as they go through these layers, that is, they change their trajectory according to Snell's law [5]

$$n_i \sin\theta_i = n_k \sin\theta_k \tag{1.2}$$

where:

$n_i$ = refraction index of medium 1
$n_k$ = refraction index of medium 2
$\theta_i$ = angle of incidence
$\theta_k$ = angle of refraction

In addition, it has been shown that the refraction index of a layer is related with the ionisation density and the frequency of the radio wave that crosses the layer by the equation [5]

$$n_i = \sqrt{1 - \frac{80.8 N_i}{f^2}} \tag{1.3}$$

where:

$n_i$ = refraction index of the layer
$N_i$ = ionisation density of the layer in $e/cm^3$
$f$ = frequency of the radio wave in Hz

So, when height increases, the refraction index decreases, which causes the radio wave to suffer more and more pronounced refractions until its trajectory becomes parallel to the Earth's surface, that is

$$n_i \sin\theta_i = n_k \sin\theta_k \tag{1.4}$$

$$n_i \sin\theta_i = n_k \sin 90^o \tag{1.5}$$

$$n_i \sin\theta_i = n_k \tag{1.6}$$

where $\theta_i$ is considered the critical angle $\theta_c$

$$\sin\theta_c = \frac{n_k}{n_i} \tag{1.7}$$

For angles of incidence higher than the critical, total reflection occurs and the radio wave returns down to Earth. On the contrary, radio waves with angles of incidence lower than the critical are refracted as they pass through the different layers until they fade away.

Anyway, the ionosphere is not a stable medium. As a consequence, we cannot consider the same critical frequency over one year or even over 24 hours. This variations will be explained in Subsection 1.1.2..

#### *1.1.1.1. D-layer*

The D-layer is the lowest layer of the ionosphere. The appearance of this region is a daytime phenomenon (it only exists during the day). At night it disappears due to recombination, the opposite process to ionisation [5].

Taking into account its electron density (specified in table 1.1) and applying the equation 1.1, it can be determined that this layer only can reflect radio waves of frequencies below 0.28 MHz, so it will not be useful for HF propagation.

Furthermore, this layer is responsible for absorbing low frequency HF radio waves, specially below 10 MHz [8]. When they pass through this layer, electrons move and collide with neutral molecules releasing their energy. Lower frequencies cause more collisions because they cause farther electron movements. In fact, the coefficient of attenuation in this layer varies as the inverse square of frequency [9].

#### *1.1.1.2. E-layer*

The following layer of the ionosphere in ascending order is the E-layer. It is also known as Kenelly-Heaviside layer and exists both day and night. Its ionisation level depends directly on solar rays and therefore it is stronger under the sun and becomes weaker at night.

Regarding ionospheric propagation, the E-layer usually reflects radio waves in the range of frequencies between 2 MHz and 4 MHz, but sometimes it can also reflect radio waves always below 10 MHz [8]. Therefore, it contributes to the absorption of higher frequencies.

**Sporadic E-layer (Es-layer)**
Sometimes, regions with a high ionisation density are formed unpredictably in the E-layer.

These regions are ionised clouds that can measure hundreds of kilometres and have large ionisation density, 10 times higher than that of the E-layer [5]. Although it is not a very useful layer since it cannot be predicted, it sometimes permits unexpected communications, as shown in Figure 1.4.

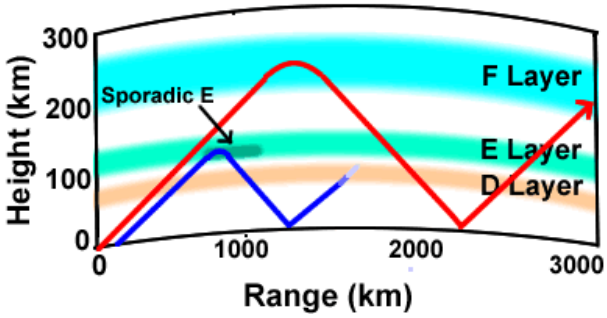


Figure 1.4: Sporadic E-layer propagation (Source: [6])

#### *1.1.1.3. F-layer*

The last region of the ionosphere is called F-layer or Appleton-Barnett layer. It extends upward from 130 km height and it has the highest electron density [10].

As it has been explained at the beginning of this section, solar rays increase the ionisation of the ionosphere during the day. Due to this, the upper part of the layer is more ionised than the lower one, and it can be considered that F layer is divided into two different layers (during the day): F1 and F2 [6].

The first one is smaller and less ionised than the second one, but its electron density is more stable. It can be considered that the appearance of the F1-layer (between 150 km and 250 km height) is a daylight phenomenon, because at night it rises and merges with F2-layer. Its behaviour is similar to the one of the E-layer although it can reflect radio waves of higher frequencies [3].

On the other hand, the F2-layer is the top layer of the ionosphere, exists both day and night and it is commonly considered the most important region for long distance HF radio communications. During the day, it exists above the F1-layer (between 250 km and 300 km height), and during the night its altitude drops to 150 km. It is believed that this layer is also influenced by the Earth's magnetic field [3]. It usually reflects radio waves with frequencies up to 10 MHz although it is considered that it can reflect higher ones if some phenomena occur in the ionosphere.

### 1.1.2. Ionosphere variations

#### *1.1.2.1. Variations due to the Solar Cycle*

Sunspots are phenomena that most affect the behaviour of the ionosphere. As the sunspot's activity is cyclical, it is referred to as solar cycle.

Sunspots are tremendous eruptions of whirling electrified gases that appear on the Sun's surface. These gases are cooled to temperatures lower than those of the surface of the

Sun and, as a consequence, dark areas appear to us as spots [3], as it can be seen in Figure 1.5.

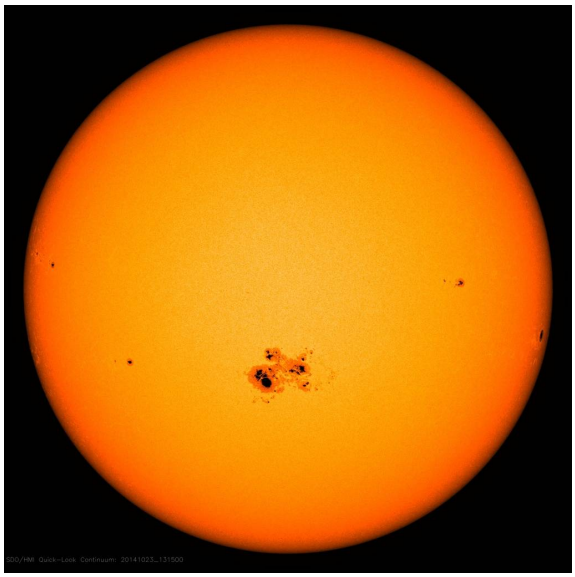

Figure 1.5: A gigantic sunspot of almost 130000 kilometres across on the Sun's surface captured in 2014 by the National Aeronautics and Space Administration (NASA) (Source: [12])

The number, intensity and duration of the sunspots is characterized by the sunspot number. It is calculated using the equation [11]

$$R = k(10g + s) \tag{1.8}$$

where:

$R =$ sunspot number
$g =$ number of sunspot groups
$s =$ number of individual spots in all the groups
$k =$ scaling factor that corrects for seeing conditions

The sunspot number is directly related to the critical frequency of the F2-layer. For example, in Figure 1.6 it can be seen how foF2 (or the critical frequency for F2-layer) grows when the sunspot number increases. On the other hand, it can also be observed how foE and foF1 are also influenced by the solar cycle but not as much as foF2. The graph shows data from the city of Canberra from 1988 to 2005, but the behaviour of critical frequencies in relation to the sunspot number can be generalized.

It is also important to note that in this case foF2 reaches frequencies of 13-14 MHz, although theoretically (according to (1.1)) F2-layer can only reflect frequencies up to 10 MHz.

#### *1.1.2.2. Seasonal variations*

The behaviour of E and F1 layers in relation to seasonal variations is really simple. We know that the ionisation of this layers depends directly on solar rays and therefore Sun's

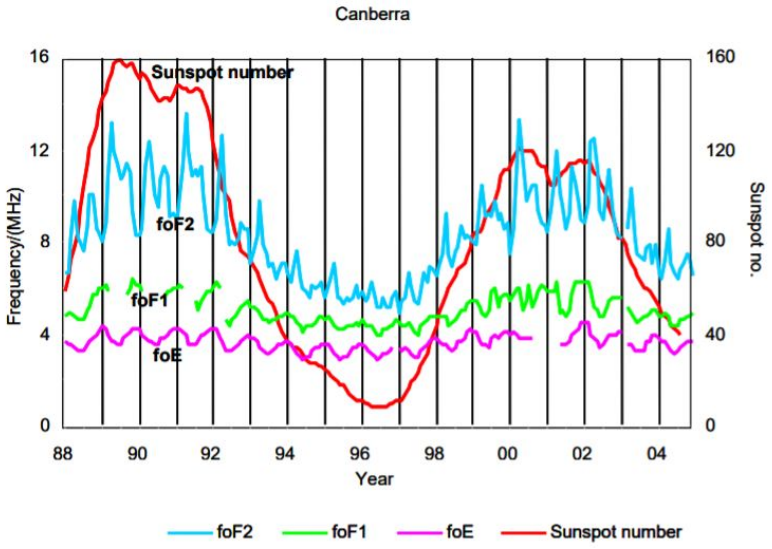


Figure 1.6: The relationship between sunspots and critical frequencies of E, F1 and F2 layers in Canberra, Australia, from 1988 to 2005 (Source: [6])

elevation affects it: it is stronger in summer than in winter [6]. Otherwise, the behaviour of F2-layer is not as simple as expected. In winter months, as a consequence of the extended periods of darkness, the ionosphere has more time to recombine and hence critical frequencies during the night dip to very low values.

On the contrary, during the summer the F2-layer heats up and expands, reducing the ionisation density to values lower than winter ones, resulting in critical frequencies also lower than the winter ones [3]. In Figure 1.6 it can be seen that foE and foF1 are greater in summer than in winter (note that data is from Australia, in the southern hemisphere), and also how foF2 decreases in summer months. It is also remarkable that foF2 peaks at March and September equinoxes (when the Sun is aligned with the earth's equator).

#### *1.1.2.3. Variations with latitude*

The intensity of solar rays that strike the ionosphere varies with latitude. Obviously, it is greater in equatorial regions than in higher latitudes. Thus, critical frequencies foE and foF1 are higher in the equator.

Moreover, foF2 is more associated with longitude than latitude (although the influence of latitude cannot be ignored). This frequency is generally higher in the Far West than in Africa, Europe and the Western Hemisphere [3].

#### *1.1.2.4. Daily variations*

Finally, we will talk about daily variations. This phenomenon is very easy to understand: critical frequencies increase during daylight and decrease during the hours of darkness. For example, foF2 reaches its maximum after the Sun has reached its zenith [3].

In transition periods that happen twice a day (once around sunrise and one around sunset), critical frequencies vary very quickly.

# CHAPTER 2. HIGH FREQUENCY COMMUNICATIONS

Once the basics of HF propagation have been explained, we can talk about more specific aspects of HF communications.

## 2.1. Amateur propagation bands

There are different frequency bands open to radio amateurs to establish communications worldwide. This frequency allocations vary from region to region, as it is defined by the ITU. In Figure 2.1 we can see three different regions:

- ITU Region 1: Europe, Africa, Northern Asia and Middle East
- ITU Region 2: North America, South America and Greenland
- ITU Region 3: East Asia and Oceania

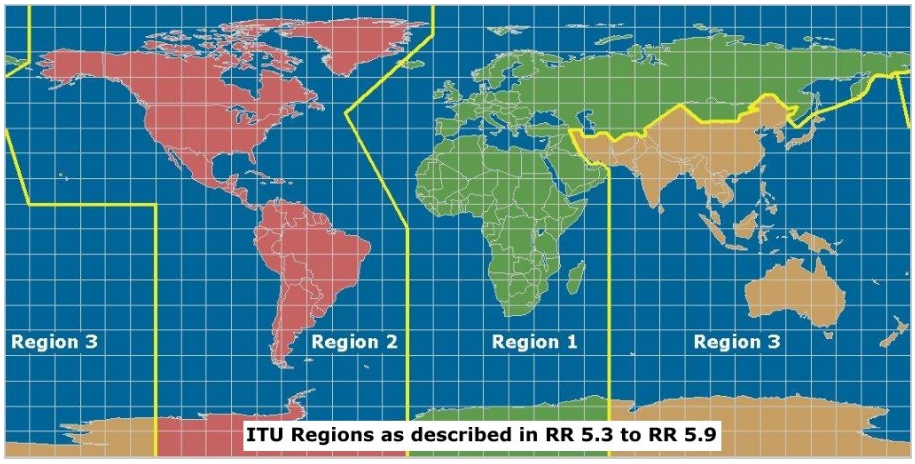


Figure 2.1: ITU regions (Source: [13])

Table 2.1 shows the different frequency ranges defined in each region for each band.

### 2.1.1. 80 meter band

This band is one of the most used by radio amateurs, especially during the night, when it offers worldwide communications. During the day, the absorption in the D-layer makes this band practically unusable and only allows local communications with high elevation angles. The upper part of this band is also known as 75 meter band [14].

### 2.1.2. 60 meter band

The 60 meter band was first introduced in 2002, but it was not until 2015 when the ITU approved a worldwide frequency allocation for it [15]. In terms of propagation, the behaviour

| Band | ITU Region 1 | ITU Region 2 | ITU Region 3 |
|---|---|---|---|
| 80 m | 3.50 MHz - 3.80 MHz | 3.50 MHz - 4.00 MHz | 3.50 MHz - 3.90 MHz |
| 60 m | 5.3515 MHz - 5.3665 MHz | | |
| 40 m | 7.00 MHz - 7.20 MHz | 7.00 MHz - 7.30 MHz | 7.00 MHz - 7.20 MHz |
| 30 m | 10.10 MHz - 10.15 MHz | | |
| 20 m | 14.00 MHz - 14.35 MHz | | |
| 17 m | 18.068 MHz - 18.168 MHz | | |
| 15 m | 21.00 MHz - 21.45 MHz | | |
| 12 m | 24.89 MHz - 24.99 MHz | | |
| 10 m | 28.00 MHz - 29.70 MHz | | |

Table 2.1: Different frequency ranges for each ITU region (Source: [16])

of this band is similar to the one of the 80 meter band but it is less affected by the D-layer absorption.

### 2.1.3. 40 meter band

The 40 meter band is one of the most reliable bands and offers worldwide communications, specially at night. As it is very popular among radio amateurs, it is a quite crowded band. In addition, although its frequency range theoretically ranges from 7.00 MHz to 7.20 MHz or 7.30 MHz (depending on the ITU region), radio amateurs can only use frequencies between 7.00 MHz and 7.100 MHz [15].

### 2.1.4. 30 meter band

The 30 meter band is one of the World Administrative Radio Conference (WARC) bands, together with 17 and 12 meter bands. They are bands reserved exclusively for radio amateurs. Its frequency range is high enough so that the size of the antennas needed to operate is quite manageable [14].

### 2.1.5. 20 meter band

This is by far the most popular HF band, especially for long distance communications. Due to its popularity, it is sometimes a bit busy, but it is also operational 24 hours a day except in cases of minimum solar cycle [5].

### 2.1.6. 17 meter band

This is one of the three WARC bands. Its behaviour is similar to that of the 20 meter band and sometimes is used by radio amateurs that want to avoid the saturation of the 20 meter band [15].

### 2.1.7. 15 meter band

This band depends a lot on solar cycles and therefore it is very variable. When radiation levels are low, it can hardly be used, but when it is high this band allows worldwide radio links with very little power. That is why it is generally used during the day. During the bottom of the sunspot cycle, this band becomes totally unusable.

In addition, it is usually open 24 hours a day in equatorial areas [5].

### 2.1.8. 12 meter band

This is the WARC band with the highest frequency and it is usually not a very busy band. It is generally used when the 10 meter band is unusable, or what is the same, when the critical frequency is below 28 MHz [15]. As the 15 meter, it is considered a daytime band.

### 2.1.9. 10 meter band

The last amateur band is the 10 meter one. It is also the wider band since it occupies 1.7 MHz. During the years of low ionisation it is rarely used, although sometimes (due to some variations in the ionosphere) it can offer long distance communications with low powers [14].

## 2.2. The Usable Frequency Range

### 2.2.1. Maximum Usable Frequency (MUF)

The Maximum Usable Frequency or MUF is the frequency located just below the critical frequency so that radio waves with equal or lower frequency will be reflected by the ionosphere [5]. It is related to the sunspot number, the date, the hour of the day or the latitude. All these things cannot be controlled by the user [3].

The difference between this frequency and the critical is that the second one is measured by emitting radio waves completely perpendicular to the Earth. Obviously, if we want to communicate using HF propagation, we are not going to emit perpendicular radio waves but obliques.

Therefore, in each layer of the ionosphere we have two possible situations [5]:

- Operating frequency $\geqslant$ MUF $\rightarrow$ The radio wave crosses the layer
- Operating frequency $<$ MUF $\rightarrow$ The radio wave is reflected

The MUF is related with the critical frequency by the secant law, as it shows Equation 2.1 [3]. Again the $f_{max}$ can be determined empirically using ionospheric sounders.

$$f_{max} = MUF \cos\theta_i = \frac{MUF}{\sec\theta_i} \tag{2.1}$$

So, the MUF can be defined as

$$MUF = f_{max} \sec \theta_i = \frac{f_{max}}{\cos \theta_i} \tag{2.2}$$

where:

$f_{max}$ = critical frequency
$MUF$ = maximum usable frequency
$\theta_i$ = angle of incidence (defined in 1.1.1.)

### 2.2.2. Lowest Usable Frequency (LUF)

The LUF is the minimum frequency that allows operation without difficulties and below which the reliability decreases to unacceptable values.

Unlike the MUF, this frequency depends on the transmitter (TX) power, the gain of the antenna or the external noise level [3].

### 2.2.3. Frequency of Optimum Transmission (FOT)

The FOT (also known as the Optimum Working Frequency or OWF) is often taken as the 85% of the MUF for the F2-layer. Working on this frequency instead of working on the MUF reduces the reception intensity but increases the stability and reliability of the communication. Due to this, the objective of any user is to keep the transmitter frequency as close to the FOT as possible [3].

### 2.2.4. Ionospheric sounders

As the ionosphere is a very variable medium, sometimes it is difficult to know exact values for critical frequencies, ionisation densities or heights of each layer.

Ionospheric sounders emit radio waves perpendicular to the earth at different frequencies to study the performance of the ionosphere. They can measure the delay between the transmission and the reception. Assuming that radio waves travel through the air at the speed of light, we can calculate the exact height where the reflection occurs. However, the measured height will not be equal to the theoretical value as the propagation speed is lower through the ionosphere. This measured height is known as virtual height [5].

The measurements made by the ionospheric sounders are shown in ionograms, as the one of Figure 2.2.

The horizontal axis shows the transmitted frequencies (from 1 to 10 MHz) and the vertical one shows the different virtual heights in km. If some ionospheric reflection is detected, it is represented with a point in the corresponding coordinates of te ionogram. Regarding to the different colours, to study the behaviour of the different ionospheric layers, we must focus in all but green ones.

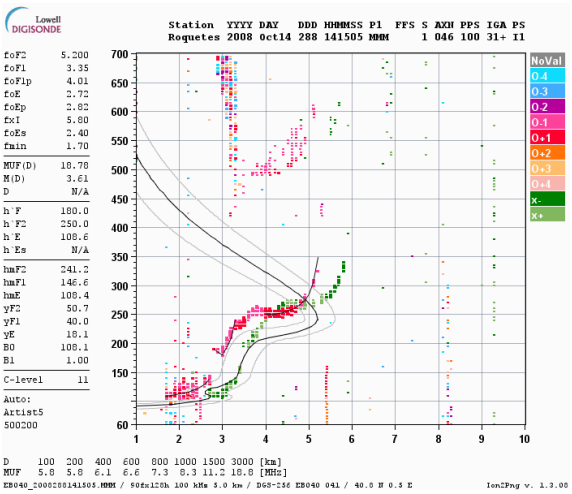


Figure 2.2: Ionogram (Source: [5])

## 2.3. Hop Length

The ground distance covered by a radio signal after one reflection on the ionosphere is called hop length. This distance depends on the elevation angle of the antenna and the height of the ionosphere layer where the reflection occurs [6]. Obviously, if the elevation angle of the antenna is higher, the radio wave will be reflected before and the hop will be shorter. The same happens when a radio wave is reflected in one of the lowest layers. This can be seen in Figure 2.3.

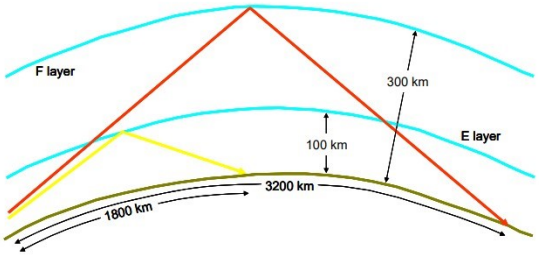


Figure 2.3: Hop lengths for two different situations (Source: [6])

In Figure 2.3, we consider heights of 100 km for the E-layer and 300km for the F-layer and an elevation angle of $4^o$ for both situations. The red radio wave will pass through layers D and E and will be reflected in the F-layer. On the contrary, the yellow signal will be reflected in the E-layer. In the first case, the hop length will be about 1800 km, and in the second one the hop length will be of 3200 km. It should be noted that when distances are big we cannot assume that the earth is flat. Considering this, calculations become complicated, and that is why the relation between the takeoff angle of the antenna and the hop length will be explained with the help of Figure 2.4.

As it can be seen, for the same takeoff angle, the higher the layer where the reflection occurs, the greater the hop length. Also, if we fix the height where the reflection is done, the smaller the takeoff angle, the greater the distance.

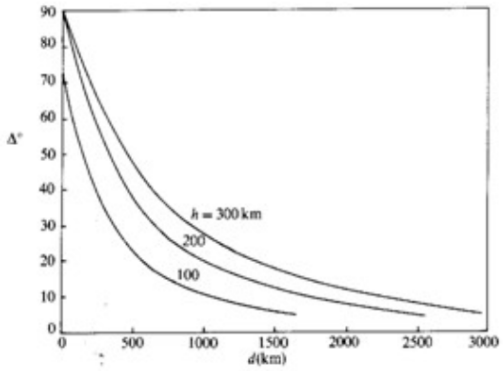


Figure 2.4: The relationship between the takeoff angle (in degrees) and the hop length (in km) (Source: [3])

## 2.4. Propagation modes

There are many ways for a radio wave to travel from the transmitter to the receiver (RX) and therefore there are different propagation modes.

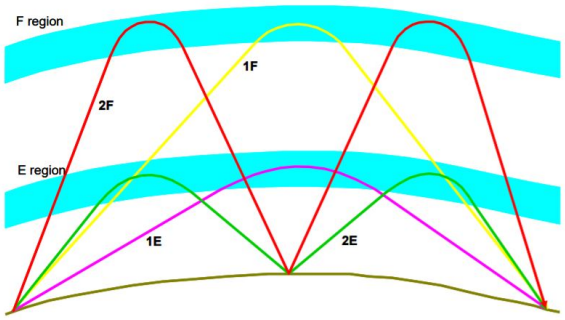


Figure 2.5: Simple propagation modes (Source: [6])

For example, when a radio wave only needs the minimum number of hops to reach the receiver, it can be considered that its propagation mode is the first order mode [6]. If the radio wave needs an extra hop, we are talking about the second order mode, if it needs two extra hops, third order mode, etc. It is important to note that the minimum number of hops is not the same as one hop. That is, if the path is of about 5000 kilometres, the minimum number of hops will be two, since with a single one it would be impossible for the radio wave to arrive.

To illustrate this, in Figure 2.5 there are represented different propagation modes. For example, the red signal represents a second order propagation mode through F-layer, that is 2F mode. On the other hand, the 1F mode is represented by the yellow line.

However, not all propagation modes are so simple. More complex modes can be seen in Figure 2.6.

If a radio wave is first reflected in the F-layer and after in the E-layer, the propagation mode will be 1F1E (pink line). If it reaches the receiver after three reflections, the first and the last one in the F-layer and the second one in the Es-layer, the mode will be 1F1Es1F (green line).

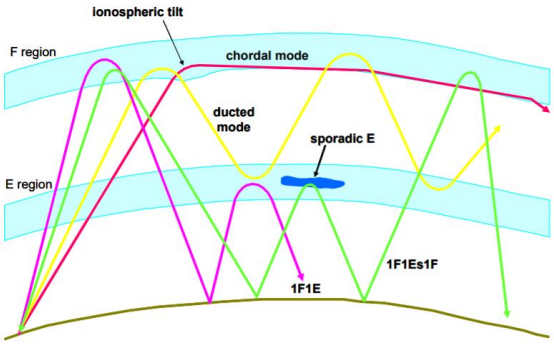


Figure 2.6: Complex propagation modes (Source: [6])

There are also two strange modes: the ducted and the chordal. Both happen when the radio wave travels from the transmitter to the receiver without intermediate reflections from the earth.

## 2.5. Noise

The noise level at the receiver has different origins, which can be internal or external to the system. The first one, also known as thermal noise, is generated in the receiver front end and it can be usually neglected. So we can consider that in HF communications external noise is by far dominant. There are four main sources [3]:

- Interference from other emitters
- Atmospheric noise
- Man-made noise
- Galactic noise

In Figure 2.7 it can be seen the variation of the external noise figure ($F_a$) of the different types of noise depending on the frequency.

The external noise figure is defined as

$$F_a = 10 \log f_a \tag{2.3}$$

where $f_a$ is the external noise factor, defined as

$$f_a = \frac{p_n}{kT_o b} \tag{2.4}$$

where:

$p_n$ = available noise power from an equivalent lossless antenna
$k$ = Boltzmann's constant in joules per kelvin (1.38e-23 J/K)
$T_o$ = reference temperature in kelvins (290 K)
$b$ = noise power bandwidth of the receiving system in Hz

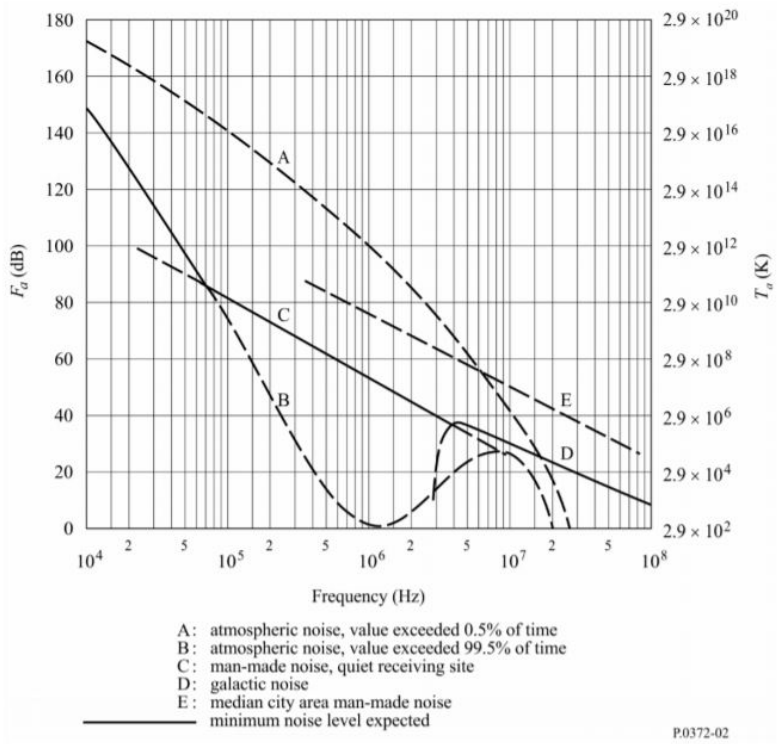


Figure 2.7: $F_a$ depending on the frequency (Source: [17])

### 2.5.1. Interference

There are tens of thousands of HF users around the world, operating in different frequency bands depending on the service they perform and the ITU region from which they emit. The best solution to mitigate interference from other users is to operate at a clear frequency where signals from other emitters are about 30 dB below the power of the desired signal [3]. This, unfortunately, is not always possible, but there are other means to overcome this problem:

- Increase the transmission power
- Use directional antennas where the interference is in a side lobe
- Use antenna nulling and create a null in the direction of the interference
- Use sharp filters on the receiver

### 2.5.2. Atmospheric noise

This type of noise is caused by thunderstorms that happen in various points of the Earth. The level of atmospheric noise is smaller in higher latitudes and greater in equatorial regions, and it obviously depends on weather conditions. In fact, it has been shown the average noise level is increased by 10 dB when there are local thunderstorms [3].

In Figure 2.7 it can be seen how atmospheric noise is the main source of noise for low frequencies, but not for higher ones. It is important to note that the dash line ”A” corre-

sponds to the atmospheric noise value that is exceeded only the 0.5% of the time and ”B” the value exceeded 99.5% of the time, so a realistic value will be between both.

### 2.5.3. Man-made noise

Man-made noise is usually predominant above 10 MHz and it is a function of industrialization and habitation density. It can be generated by many sources, such as industry, electrical machinery, power transmission lines or electrical cables [6] [4].

The median value of its external noise figure ($F_{am}$) can be calculated with the following equation

$$F_{am} = c - d \log f[MHz] \tag{2.5}$$

where $c$ and $d$ are values that depend on the environmental categories and can be taken from Table 2.2. There are 4 different categories defined by the ITU: city, residential, rural and quiet rural.

| Environmental category | c | d |
|---|---|---|
| City | 76.8 | 27.7 |
| Residential | 72.5 | 27.7 |
| Rural | 67.2 | 27.7 |
| Quiet rural | 53.6 | 28.6 |

Table 2.2: Environmental categories defined by the ITU (Sources: [3])

City areas are defined as those where there is any type of business (like offices, stores, shopping centres, main streets or industrial parks). On the other hand, residential areas are those where we can find at least five family residences per hectare and without busy highways, unlike rural areas, where family units are limited to five per hectare. Finally, we have quiet rural areas which correspond to remote areas [17].

Also, Figure 2.8 can help us to understand how every type of noise varies depending on the frequency. In all cases, if the frequency increases, the noise power decreases.

To mitigate the effects of man-made noise, it will be a good option to use directional antennas (specially in reception). On the other hand, man-made noise has usually a vertical polarisation [6], so choosing an antenna with horizontal polarisation will also help.

### 2.5.4. Galactic noise

This type of noise is originated outside the atmosphere, in our galaxy [6]. It is considered that it only influences high frequencies and, as it can be seen in Figure 2.8, it is only relevant above 10 MHz (see ”E” dash line).

In the frequency range of HF propagation, the median noise figure for galactic noise can be calculated with the equation 2.6, where $f$ is the frequency of operation expressed in MHz.

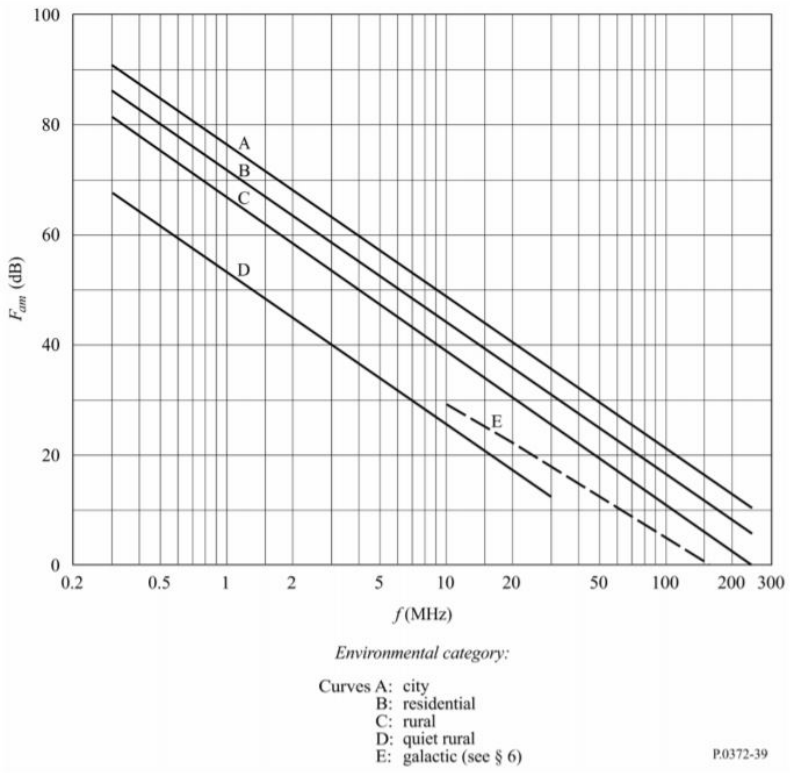


Figure 2.8: Median values of man-made noise power (Source: [17])

$$F_{am} = 52 - 23 \log f \tag{2.6}$$

# CHAPTER 3. HIGH FREQUENCY TRADING

## 3.1. Introduction

High-frequency trading or HFT is a form of automated trading that employs [18]:

- Powerful computers
- Algorithms for each individual transaction without human direction
- Low-latency technology designed to minimize response times
- High-speed connections
- High message rates

Though it may seem something innovative, we are aware of the existence of HFT since 1998, when the Securities and Exchange Commission (SEC) of the United States authorized electronic exchanges. Before this event, stock trading was very simple: buyers and sellers met in exchange houses and negotiated until reaching an agreement.

Between 2009 and 2010, HFT transactions accounted for around 60% of all trading volume in the United States (see Figure 3.1). This percentage was lower in Europe, around 30-40%. Even so, it is a stock market trend generally unknown [19].

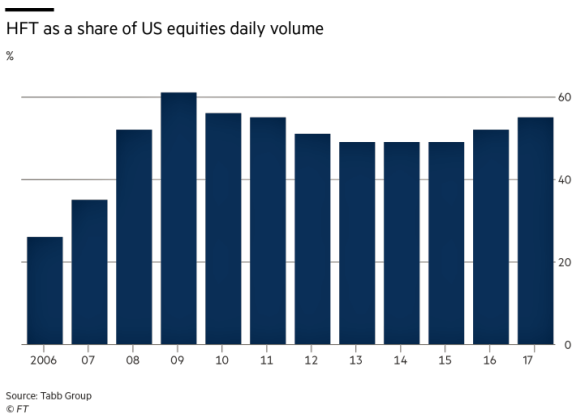


Figure 3.1: HFT as a share of United States (US) equities daily volume (Source: [20])

The general practice of high frequency traders is based on launching trade orders to the market and cancel them before they are carried out. As HFT systems have faster processing speeds than others, they are allowed to see the actions of the other operators before and act accordingly [21].

A good example will be the following:

An operator offers shares at a certain price. Thanks to the high processing speed, the system can see if another operator has issued a purchase order with enough time to cancel the sale order. But, why does the operator want to cancel the sale? It is very simple. Knowing that there is a buyer interested in the shares, the operator will repeat the

same operation increasing in each iteration the price of the shares until discovering the maximum price for which the other operator is programmed to buy. Thus, the operator will sell all the shares taking the maximum possible benefit.

It may seem that the benefit obtained with these transactions is small, but if we take into account that this can be repeated thousands of times every second, benefit throughout the day will be high.

In Figure 3.2 it can be seen the daily comparison between quotes and trades for US stocks. The red line shows the number of quotes, which are defined as unrealized transactions, unlike the blue line, which shows realized ones.

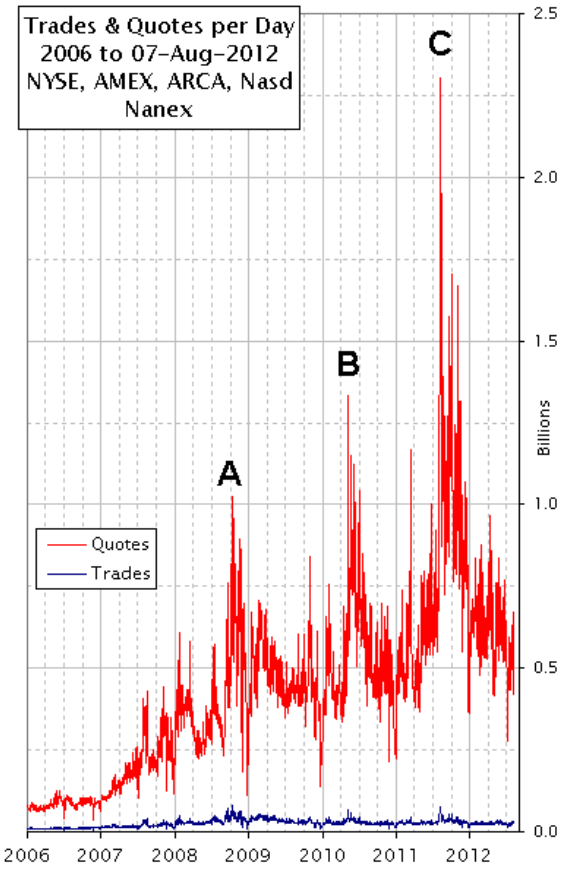


Figure 3.2: Comparison between trades and quotes from 2006 to 2012 (Source: [22])

The difference between the two draws attention (note the scale is in billions). The three peaks (labeled as A, B and C) of the graph are also remarkable as they show the moments when the difference between quotes and trades has been larger [22]:

**A** Financial Crisis of 2008

**B** Flash Crash of 2010

**C** US Downgrade of 2011

This highlights the importance and relevance of High Frequency Trading in the stock markets and in the global economy.

## 3.2. The importance of HF Propagation in HFT

The advantage of a few milliseconds in the field of trading stock markets is evident, and that is why many financial firms have begun to look for alternatives to reduce latency. When we think about reducing the latency of a link, the first question that we must ask ourselves is: how can we make information travel faster?

It is in this context when the possibility of establishing a HF radio link comes to mind. It is obvious that information propagates faster through the vacuum than through an optical fiber as the refractive index of silica (the material from which the fiber core is generally made) is larger than the one of the vacuum. Concretely, the mean refraction index value of silica is 1.458 [23]. A greater refraction index means a lower speed through the medium, as

$$n = \frac{c}{v} \tag{3.1}$$

and so [23]

$$v = \frac{c}{n} \tag{3.2}$$

where:

$n =$ refraction index of a medium
$c =$ speed of light through the vacuum in m/s
$v =$ speed of light through the medium in m/s

If we substitute the refractive index variable in equation 3.2 and put the corresponding values for air (not vacuum) and silica, we will get:

$$v_{air} = \frac{3 \cdot 10^8}{1.00027} = 2.999 \cdot 10^8 [m/s] \tag{3.3}$$

and

$$v_{fiber} = \frac{3 \cdot 10^8}{1.458} = 2.058 \cdot 10^8 [m/s] \tag{3.4}$$

Although the refraction index of the air is not exactly the same as the one of the vacuum, the difference is inappreciable. Now, if we compare both results we can say that the speed of light through an optical fiber is practically 2/3 of the speed through the air:

$$v_{fiber} \cdot n_{fiber} = v_{air} \cdot n_{air} \tag{3.5}$$

$$v_{fiber} = \frac{v_{air} \cdot n_{air}}{n_{fiber}} \tag{3.6}$$

$$v_{fiber} = \frac{1.00027}{1.458} v_{air} \tag{3.7}$$

$$v_{fiber} = 0.686 v_{air} \simeq \frac{2}{3} v_{air} \tag{3.8}$$

Anyway, the comparison between fiber optic and HF links is going to be analysed in Chapter 7.

All this evidence has made many companies as IMC BV investigate and test shortwave links [1]. We are certain that this is happening because every microwave link requires a license to operate, and this experimental licenses are public data that can be checked.

In any case, it is hard to find information about these links (such as the working frequency or the protocol used) because companies compete with each other to get the lowest latency. A good example to illustrate this is the following antenna, located in Wesley Hills, New York.

Figure 3.3: Camouflaged antenna in Wesley Hills, New York (Source: [24])

As it can be seen, the antenna is very well camouflaged and from a distance it can look like a simple tree.

# CHAPTER 4. LINK

## 4.1. Basic description

The basic structure of our bidirectional link is shown in Figure 4.1. As we know, as the link is bidirectional, both stations transmit and receive information.

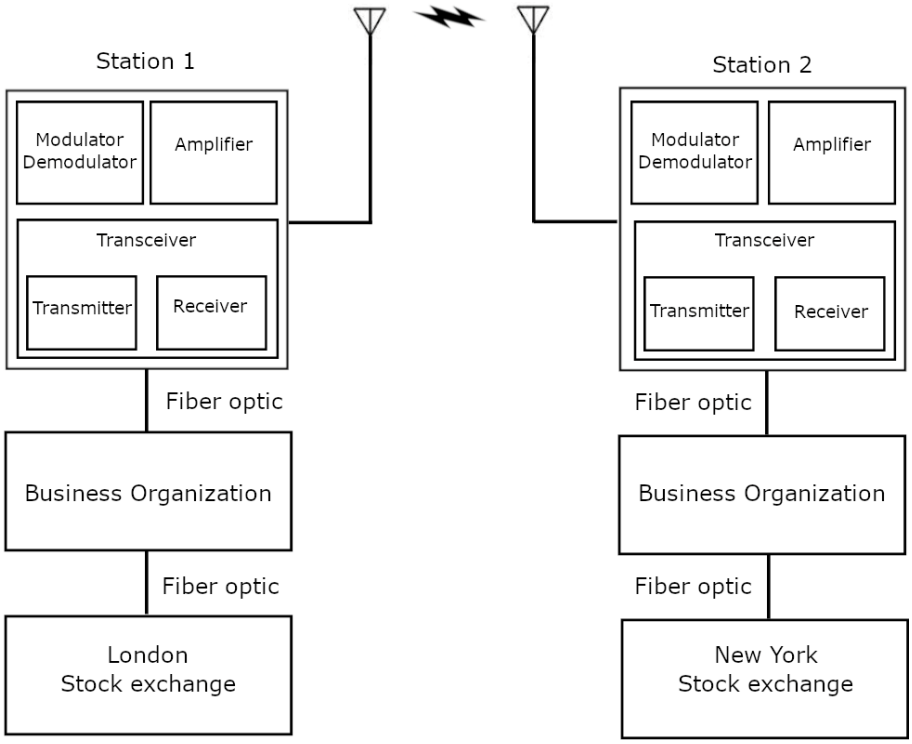


Figure 4.1: Basic structure of our system

As it can be seen, both stations have three basic blocks:

1. Modulator / Demodulator
2. Amplifier
3. Transceiver (a device which comprises a transmitter and a receiver)

Although the transatlantic connection between sites will be done through HF propagation, the link between them, business organisations and stock markets will be done with optical fibers. One of the basic requirements to establish a shortwave link is that sites have to be located in noise free areas, so if we place a receiving antenna in the city center we won't be able to demodulate the received signal correctly.

## 4.2. Sites location

The first thing we have to decide is where we are going to place our sites. As we know, our bidirectional link will connect the United States of America with the United Kingdom, in particular New York and London, which have important stock exchanges.

The most important thing we have to take into account when choosing the location of the sites is to make sure they are low noise areas.

### 4.2.1. US site

For the United States, we have chosen the outskirts of the hamlet of Riverside, in Suffolk County (New York). This site is mentioned in some Internet forums [26] and it has an experimental shortwave license on behalf of a company called Skycast Services [27]. Skycast Services, as it is explained in its website, is "a specialized R&D firm that develops and commercializes creative telecommunication solutions for clients around the world" [28]. So, if there is a company testing this type of technology in this particular place, it will be probably a good area to install our antenna there.

Concretely, the US site is situated at coordinates 40° 52' 54.3" N 72° 38' 14.9" W.

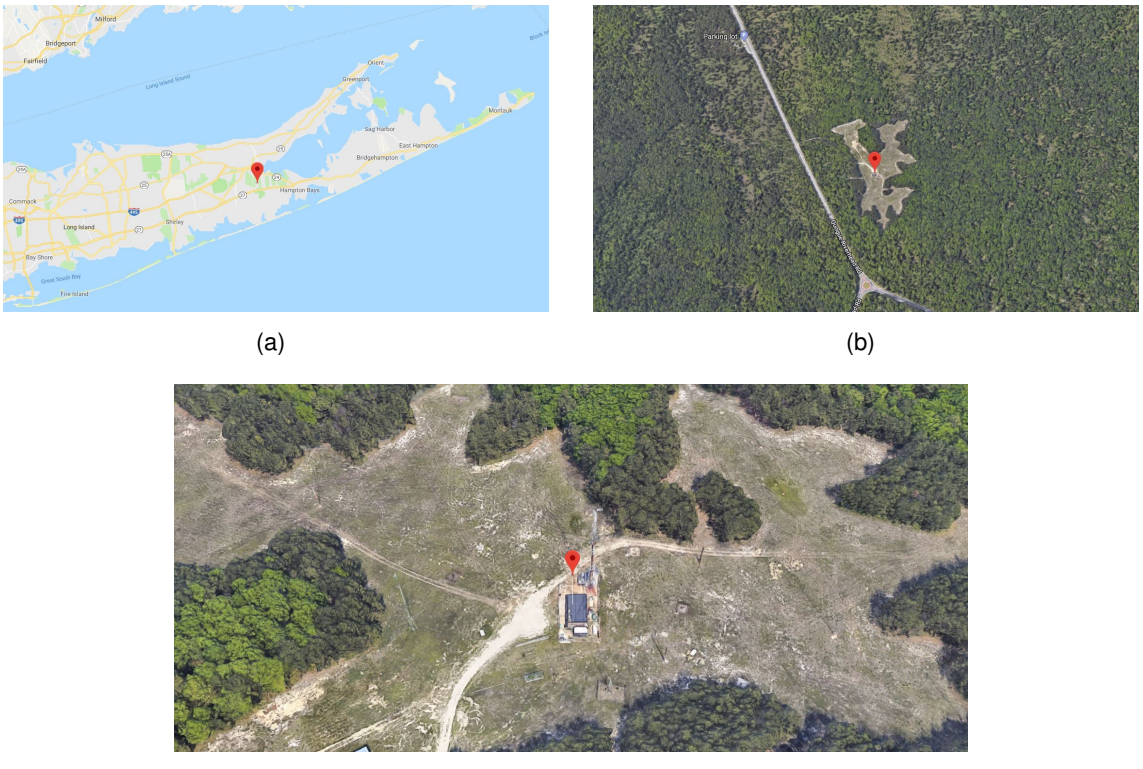


(a) (b)

(c)

Figure 4.2: Google Maps screenshots of the location of the US site

This choice is due to the proximity of the site to New York considering that the area is practically uninhabited. In Figure 4.2 (b) it can be seen that the area is really remote and therefore noise free.

The exact distance between the site and the New York Stock Exchange is 118.63 kilometres, as it can be seen in Figure 4.3.

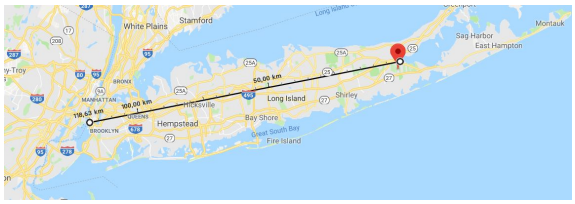


Figure 4.3: Google Maps screenshot of the distance between the site and New York

### 4.2.2. UK site

On the other hand, the United Kingdom site will be located on the outskirts of the city of Bude, in the north east Cornwall. Again, the Internet has been essential to choose this site. In this small city it is situated a satellite ground station and eavesdropping centre of the UK Government, so it can be deduced that it is a good location to install our site.

Concretely, it will be situated at coordinates 50° 52’ 26.1” N 4° 33’ 17.5” W.

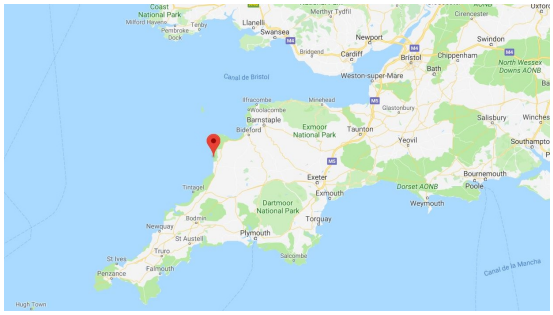


(a)

(b)

Figure 4.4: Google Maps screenshots of the location of the UK site

In this case, it is 318.54 kilometres away from the London Stock Exchange, as we have measured using Google Maps (see Figure 4.5).

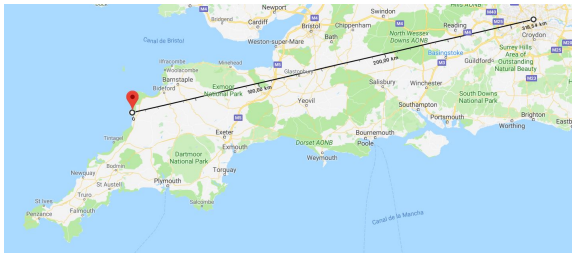


Figure 4.5: Google Maps screenshot of the distance between the site and London

## 4.3. Antennas

After deciding where we are going to locate our sites, the next question is: which type of antenna are we going to use?

There are lots of different types of antennas typically used in HF communications: rhombic antennas, the log-periodic antenna family, dipoles, broadband vertical antennas, Yagi-Uda antennas, etc.

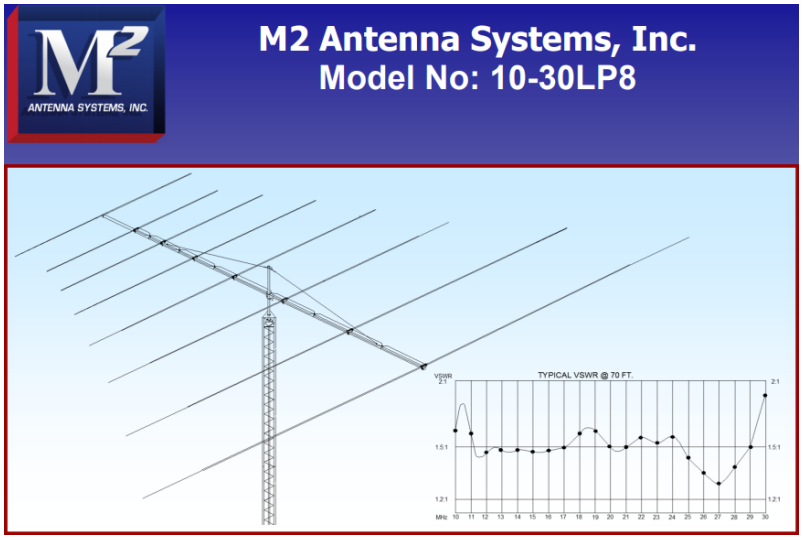


(a)

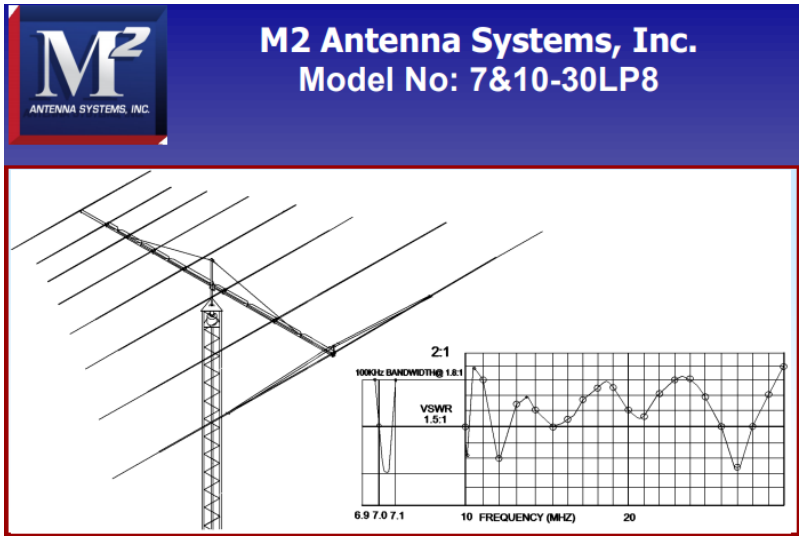


(b)

Figure 4.6: 10-30LP8 and 7&10-30LP8 antennas

For our link, we are going to use a log-periodic antenna. This choice has been based on a patent for “Data transmission via a high frequency radio band” [25]. In this patent two antennas of the manufacturer M2 Antennas Systems, Inc. are proposed: 10-30LP8 [29] and 7&10-30LP8 [30]. Both are 8 element log-periodic antennas and have practically the same specifications (see Table 4.1).

Within the group of log-periodic antennas, 10-30LP8 and 7&10-30LP8 have a dipole array structure (see Figure 4.7), one of the most common configurations for this type of antenna.

| Model | 10-30LP8 | 7&10-30LP8 |
|---|---|---|
| **Frequency range** | 10-30 MHz Continuous | 10-30 MHz Continuous and a separate frequency tunable 6.6 - 8 MHz |
| **Gain free space** | 5.2 dBi / 10.5 dBi 10-30 MHz | 5.2 dBi / 10.5 dBi 10-30 MHz and 2 dBi / 6.5 dBi 6.6-8 MHz |
| **Front to back** | 15 dB 10-30 MHz | |
| **Beamwidth** | E = 70 degrees | |
| **Feed Impedance** | 50 Ohms | |
| **Maximum VSWR** | 2:1 | |

Table 4.1: Specification comparison between 10-30LP8 and 7&10-30LP8 antennas (Source: [29] [30])

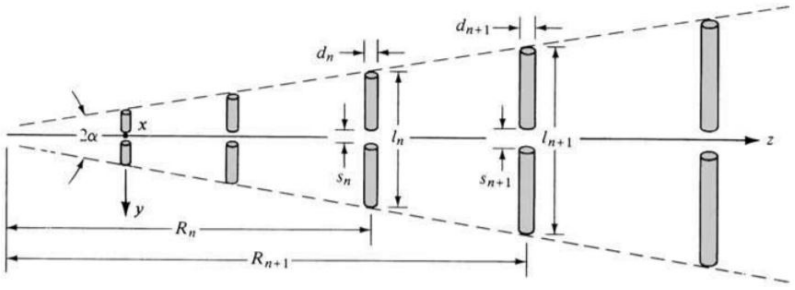


Figure 4.7: Log-periodic dipole array structure (Source: [31])

Although it may seem similar to a Yagi-Uda array, they have a lot of differences. On the one hand, they are less directional but they can work across wider frequency ranges. Usually, Yagi-Uda antennas are designed to work on a concrete small range of frequencies. On the other hand, contrary to what happens with Yagi-Uda arrays, the dimensions of elements follow a geometric ratio $\tau$, defined in equation 4.1. Also, its name comes from the fact that the spacing between elements follow a logarithmic function [31].

$$\frac{1}{\tau} = \frac{l_{n+1}}{l_n} = \frac{R_{n+1}}{R_n} = \frac{d_{n+1}}{d_n} = \frac{s_{n+1}}{s_n} \tag{4.1}$$

Where:

$\tau$ = geometric ratio
$l_n$ = length of the elements
$R_n$ = spacing between elements
$d_n$ = diameter of the elements
$s_n$ = gap spacing at dipole centers

Another difference between Yagi-Uda and log-periodic antennas is that in the former only one of the elements is electrically fed. It is known as the active ot driven element. On the contrary, in log-periodic arrays all elements are connected. Figure 4.8 shows the main methods used to feed all the elements of the array:

Regarding 10-30LP8 and 7&10-30LP8 antennas, both are connected by a straight connection, as shows Figure 4.8 (a).

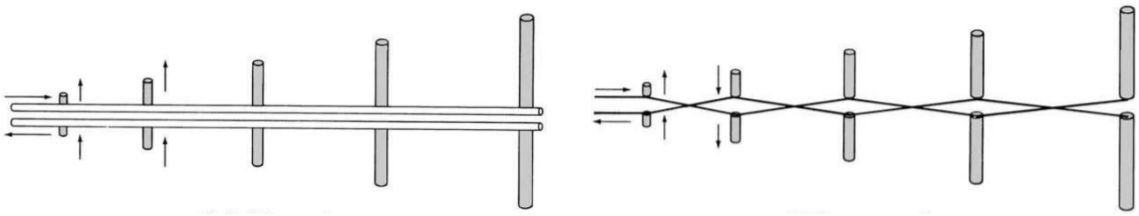

(a) Straight connection (b) Crisscross connection

Figure 4.8: Main connection methods for log-periodic arrays

As Table 4.1 shows, the most important difference between them is that the second one has a separate frequency tunable from 6.6 to 8.0 MHz. This means that this antenna can operate on 40, 30, 20, 17, 15, 12 and 10 meter bands. On the other hand, the first antenna can only operate on the six lowest bands. In addition, 80 and 60 meter bands will be discarded in both cases.

Another important difference between both antennas is the VSWR (Voltage Standing Wave Ratio). This parameter is related to the impedance matching between the antenna and the transmission line that feeds it and it can be defined as [32]:

$$VSWR = \frac{1+|\Gamma|}{1-|\Gamma|} \tag{4.2}$$

where $\Gamma$ is the reflection coefficient of the antenna.

The ideal case is when impedances are perfectly matched and there is no reflected power from the antenna. If this happens, the VSWR will be 1:1. So, the higher the VSWR, the higher the return losses. Table 4.2 can help us to understand the correlation between the VSWR and the percentage of reflected power.

| VSWR | Returned power (approximate) |
|---|---|
| 1:1 | 0% |
| 2:1 | 10% |
| 3:1 | 25% |
| 6:1 | 50% |
| 10:1 | 65% |

Table 4.2: Correlation between VSWR and the percentage of returned power (Source: [33])

Figure 4.6 shows the change with frequency of the VSWR of both antennas. At first glance it can be seen that, in general, the VSWR of the 10-30LP8 antenna is lower than the one of the 7&10-30LP8, so its performance will be better.

However, taking into account the simulation results in Chapter 6, the chosen antenna will be the 7&10-30LP8, as one of the most reliable bands is the 40 meter band.

## 4.4. Protocol and modulation

There are different protocols used by radio amateurs to communicate between them. In our case, conditions are a bit different. We need above all a protocol that works with a noise-resistant modulation to ensure high reliability. After all, the advantage of establishing this link is the reduction of latency, but this would be useless if we cannot provide reliable communication throughout the year.

Considering this, we will opt for a digital frequency modulation. The most common protocols using Frequency Shift Keying (FSK) modulations are shown in Table :

| Protocol | Modulation |
|---|---|
| WSPR | 4FSK |
| FT8 | 8FSK |
| FT4 | 4GFSK |

Table 4.3: Radio amateur protocols and its modulations (Sources: [34] [35] [36])

First of all, we compare the 8 symbol modulation (8FSK) with 4FSK and a 4 symbol Gaussian Frequency Shift Keying (GFSK) modulation. Obviously, if we choose 8FSK we will be able to transmit more information, but the signal will be less resistant to intersymbol interference(ISI) because the distance between symbols will decrease [37]. At this point, we have to make a decision: prioritize the reliability of the link or its capacity. As we have explained, our goal is to establish a link with low latency and high reliability, so we will discard 8FSK modulation.

Now we have to decide between 4FSK and 4GFSK. The approach is similar: prioritize the reliability above all. In Figure 4.9, it can be seen how in the spectrum of the FSK modulation there are unwanted spurious components and high side lobes. On the contrary, the spectrum of GFSK modulation has not this spurs and side lobes, as a Gaussian filter is applied to the symbols before modulating the signal.

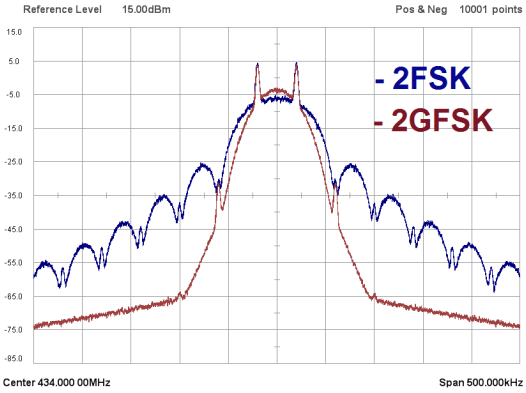


Figure 4.9: Comparison between 2FSK and 2GFSK spectra (Source: [37])

Despite these advantages, the sensitivity of the receiver is reduced and therefore the reliability is also reduced [37]. As we have already explained, we want the highest possible reliability, so we will choose the Weak Signal Propagation Reporter (WSPR) protocol.

## 4.5. Transmitted power

To choose the transmitted power for our link, we have also consulted the patent of the previous section, where a power of 100 watts is proposed [25]. Still, greater power levels are also contemplated if necessary.

On the other hand, there is another interesting document on the return of HF propagation in relation to High Frequency Trading. It talks about a startup called Shortwave Traders that is testing a HF link between Frankfurt (Germany) and New York. Its technical director, Andrej Pramen, explains that they are using transmission powers of 2000 watts [38].

In conclusion, the idea is to obtain high reliability using the minimum possible power and so reducing the cost of the link. Concretely, we will try to make the link work with a transmitted power of 200 watts but it will be considered the option of increasing the power level if necessary.

## 4.6. Number of hops

The distance between the TX and the RX is of about 5200 km. This means that we will need at least 2 hops of 2600 km. In reference to the explanation in Section 2.3., if the radio wave is reflected on the upper part of the F-layer, with a small takeoff angle (of less than 10 degrees) we will need a maximum of two hops. On the contrary, if the reflection is done in the lower part of the F-layer, we will need at least 3 different hops if the take off angle is approximately 10 degrees. In this case, each hop will be of 1750 km. Finally, if the reflection occurs in the E-layer, the radio wave will hop a minimum of 4 times before reaching the receiver.

Obviously, the best situation will be that the reflections of the radio wave occur in the F2-layer, as the distance of the path will be lower, as well as the attenuation of the signal. So, the desired propagation mode for our path will be the first order mode 1F2 (as the minimum hop number is 2).

# CHAPTER 5. VOACAP SOFTWARE

As it has been explained, the ionosphere is not a stable medium, and it will be practically impossible to predict the behaviour of a HF link without any software. In our case, the software used to make the simulations of this communication is an online website called Voice of America Coverage Analysis Program (VOACAP) (www.voacap.com/hf).

VOACAP is a HF propagation prediction software that allows users to simulate communications between two points of the Earth [39]. It gives very valuable information about the link reliability depending on the working frequency. This software is normally used by radio amateurs who want to test if their transmissions will be successful or if they have to make some adjustments.

This chapter will focus on explaining the main features of this software and the different inputs that we are going to introduce to simulate our link.

## 5.1. Software inputs

When you access the website, the first thing you see is the following screen:

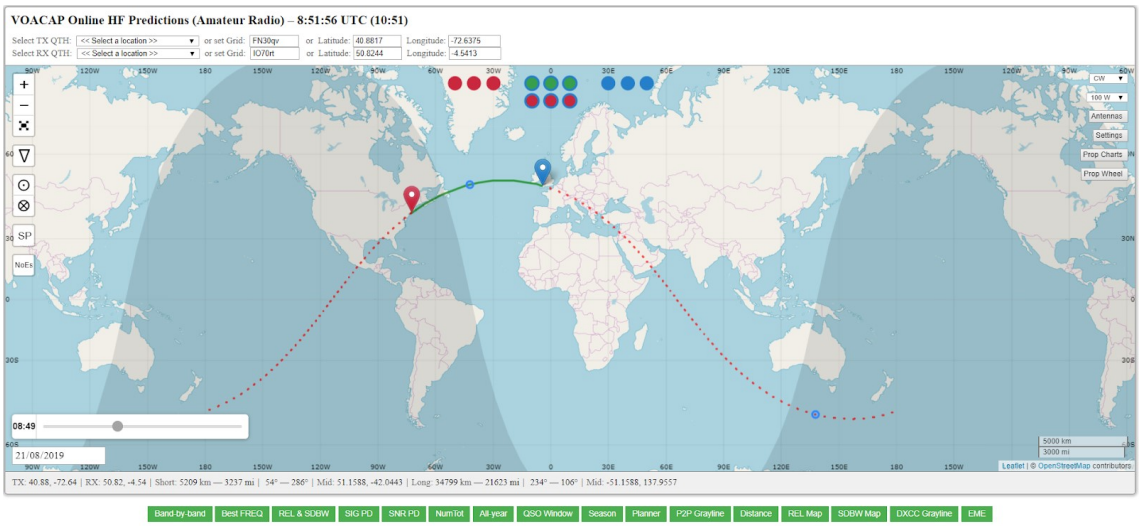


Figure 5.1: VOACAP's main map (Source: [40])

### 5.1.1. TX and RX location

First of all, the location of both transmitter and receiver has to be chosen. In our case, as it has been explained in Chapter 4, the link is bidirectional, so it does not matter which station is the transmitter (red marker) and which is the receiver (blue marker). Green line between stations shows the short path and the dotted red line the long path. In both cases, the small blue circles indicate the geographical midpoint of the link [41].

For instance, we decide to locate the transmitter in the United States and the receiver in the United Kingdom, as it can be seen in Figure 5.1.

### 5.1.2. Day and hour

As VOACAP is a prediction software, links can be tested at different dates. At bottom left corner of the screen we can choose a particular hour and date. If we change the hour, it can be seen how the shadowed region moves through the map. On the other hand, regarding to the date, it is important to note that VOACAP makes month predictions, that is, the results will be the same if we test the link choosing de first or the last day of the same month.

In our case we are going to simulate the link from January to December of 2020.

### 5.1.3. Transmitting Mode menu

At top right of the screen there are different pop-up menus and buttons. The first one (from top to bottom) is the Transmitting Mode menu, where we can choose between WSPR, FT8, FT4, Continuous Wave (CW), Single Side Band (SSB) and Amplitude Modulation (AM) protocols [40]. For our link, as it has been explained in Chapter 4, the best option is WSPR protocol.

### 5.1.4. Transmitting Power menu

In this menu we can choose the transmitting power, from 0.1 W to 1500 W. The power that uses the software for the calculations is 80% of the power chosen due to the line losses [41].

In our case, we decided to use a power of 100 W and increase if necessary, as explained in Section 4.5.. The maximum power level that we consider is 2000 W. So the power chosen in this menu should be between $P_{min}$ and $P_{max}$. First we calculate $P_{min}$.

$$\frac{80}{100}P_{min} = 100W \tag{5.1}$$

and so

$$P_{min} = \frac{100 \cdot 100}{80} = 125W \tag{5.2}$$

As this power is not in the given options, we choose a higher value of 200 W to achieve the required power.

Now, we calculate $P_{max}$:

$$\frac{80}{100}P_{max} = 2000W \tag{5.3}$$

and so

$$P_{max} = \frac{2000 \cdot 100}{80} = 2500W \tag{5.4}$$

Again, this power is not in the given options. In fact, the maximum power that VOACAP offers is 1500 W, so our power range will be between 200 W and 1500 W.

### 5.1.5. Antennas button

VOACAP offers different types of antennas for the transmitter and the receiver. For example, yagis of variable number of elements, dipoles, isotropic antennas... also working at different frequency bands [40].

In Section 4.3. we have chosen a log-periodic antenna for both the transmitter and the receiver, but VOACAP does not make simulations with this type of antenna. In this case, the most similar is a Yagi-Uda. The problem is that these type of antennas are usually designed to work on small ranges of frequencies. For example, we can find in VOACAP a 10M 3 element Yagi. This antenna is designed to work exclusively on the 10 meter band and it will not be a good option to work on other frequencies.

To try to make a realistic simulation, we will opt to use different Yagi antennas (designed to work on different amateur bands) to simulate the behaviour of a log-periodic antenna. To understand this better, see Table 5.1.

| | |
|---|---|
| **40 M** | 8-element Yagi 40M |
| **30 M** | 8-element Yagi 30M |
| **20 M** | 8-element Yagi 20M |
| **17 M** | 8-element Yagi 15M |
| **15 M** | 8-element Yagi 15M |
| **12 M** | 8-element Yagi 10M |
| **10 M** | 8-element Yagi 10M |

Table 5.1: Antennas chosen for each band

### 5.1.6. Settings button

This button shows a menu where there are three parameter sections. The most important settings are the following:

#### *5.1.6.1. Noise*

Here we have to select the noise level at the receiver site. There are different options: Noisy, Industrial, Residential, Rural, Quiet and Remote [40]. Our antennas are both placed in rural areas, far from big cities where noise level is higher, so we select Rural noise level.

#### *5.1.6.2. Smoothed Sunspot Number (SSN)*

As explained in Chapter 1, sunspots can be counted using the sunspot number. Even so, VOACAP works with a similar number called smoothed sunspot number.

VOACAP offers two options to set this value: either introducing manually a particular SSN or using the software prediction (in this case -1 value has to be introduced). The predictions

are based on the Lincoln-McNish smoothing function, and they are done by the Sunspot Index and Long-term Solar Observations (SILSO) of the Royal Observatory of Belgium in Brussels [41].

Figure 5.2 shows the sunspot number for 2015 to now and the prediction (based on the Lincoln-McNish smoothing method) for the next months. It can be seen that we are currently on the bottom of the sunspot cycle.

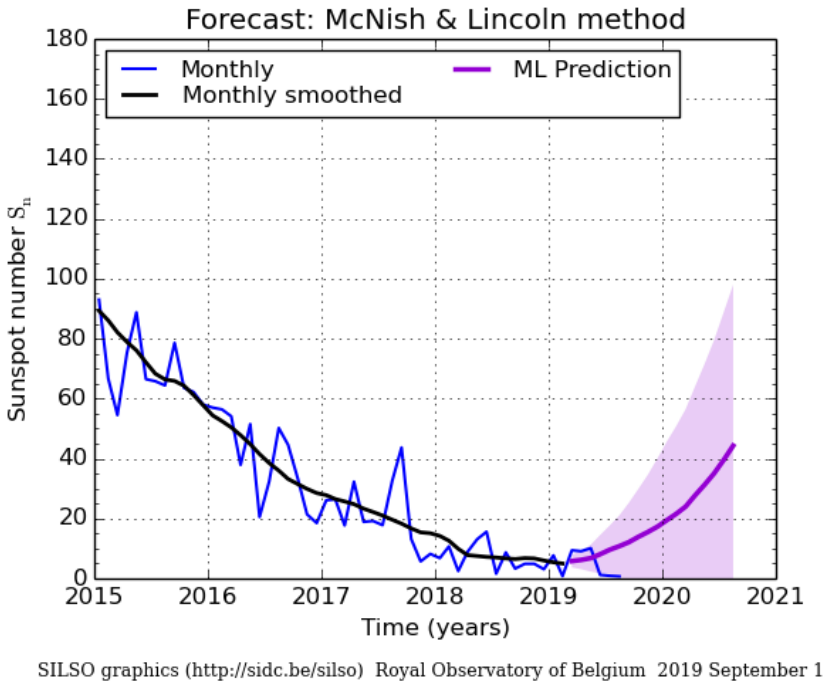


Figure 5.2: SSN (Source: [42])

For our radio link, we will use the “-1” option.

#### *5.1.6.3. Method*

With this menu users can choose the propagation model that VOACAP will use to do the simulations. There are 3 options: Auto, Ducted and Ray-hop. The choice of the propagation model is mainly based on the transmission distance. The Ducted model is typically used for paths of 10.000 km, while the Ray-hop model is used for paths less than 10.000 km [41].

As it has been explained in Chapter 4, the distance between the transmitter and the receiver is about 5200 km, so we will use the Ray-hop model.

#### *5.1.6.4. Minimum Takeoff Angle (TOA)*

Finally, the last parameter we have to set is the minimum takeoff angle or the elevation angle for our antennas. A value of 3 degrees is usually recommended [41], so this will be our choice. It is important to consider that, as our link is bidirectional, this angle will be the same both in transmission and in reception.

It is important to note that this value is the minimum, but it can be increased if necessary. VOACAP changes automatically this value to get high reliability levels. As explained in Chapter 4, the maximum TOA will be 10 degrees if we want a 1F2 propagation mode. Regarding to our link, it will be interesting to change the elevation angle of the antenna automatically following some kind of algorithm.

In Table 5.2, all input parameters are synthesized.

| | |
|---|---|
| **TX location** | 40° 52' 54.3" N 72° 38' 14.9" W |
| **RX location** | 50° 52' 26.1" N 4° 33' 17.5" W |
| **Transmitting power** | 200 W - 1500 W |
| **Antenna** | See 5.1.5. |
| **Noise** | Rural |
| **SSN** | -1 |
| **Method** | Ray-hop model |
| **Minimum TOA** | 3° |

Table 5.2: Input parameters for the simulations

## 5.2. Software outputs

VOACAP offers a lot of data about the performance of the tested transmission. For our study, there are three different charts that will be really useful.

In all of them, the hours of the day are expressed at a longitude of 0 degrees following the Coordinated Universal Time (UTC) standard. As our receiver is located in the United Kingdom, we will have to add one hour from the one shown in the chart to analyse the performance of the link.

### 5.2.1. Circuit Reliability chart

This chart shows the circuit reliability factor, that is the percentage of days in the month when the simulated Signal-to-Noise Ratio (SNR) exceeds the required SNR [41], an internal value setted by VOACAP related to the protocol (and modulation) used.

In Figure 5.3 it can be seen how it looks like. In the vertical axis we have the probability of success and in the horizontal we have the different hours of the day. Every amateur band is represented with a different colour. Also, VOACAP offers an unusual amateur band, the 11 meter band.

At this point we have to decide which is the minimum reliability accepted to consider that a circuit is reliable. For example, although it may seem a high value, a 80% means that the link is not going to work 6 out of 30 days of a month. Obviously, we cannot accept this, so the minimum reliability will be setted at a 95% (the link is not going to work approximately 1 out of 30 days).

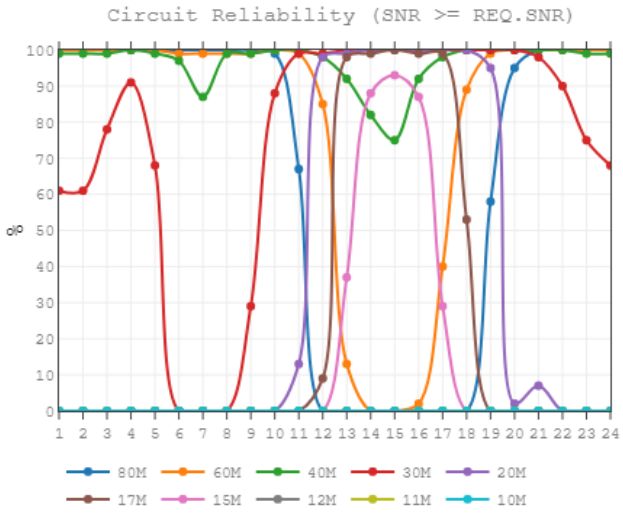


Figure 5.3: Reliability chart (Source: [40])

### 5.2.2. 24-hour propagation prediction wheel

This wheel displays the reliability parameter in a more visual way. Each circle represents one of the nine amateur bands, and each section one of the hours of the day.

### 5.2.3. SDBW chart

The signal power distribution shows the level of power (in dBW) that can be maintained on 50% of the days in one month, working on a concrete frequency at a given hour [41].

Again, every amateur band is represented with a different colour. In the vertical axis we have the power level and in the horizontal the hours of the day.

In this chart, the power is represented by the S-meter scale. In Table 5.3 it is shown the relation between each S-meter point and its power (expressed in dBm and Watt).

| S-meter point | Power (dBW) |
|---|---|
| S9 | -103 |
| S8 | -109 |
| S7 | -115 |
| S6 | -121 |
| S5 | -127 |
| S4 | -133 |
| S3 | -139 |
| S2 | -145 |
| S1 | -151 |
| S0 | -157 |

Table 5.3: S-meter scale (Source: [41])

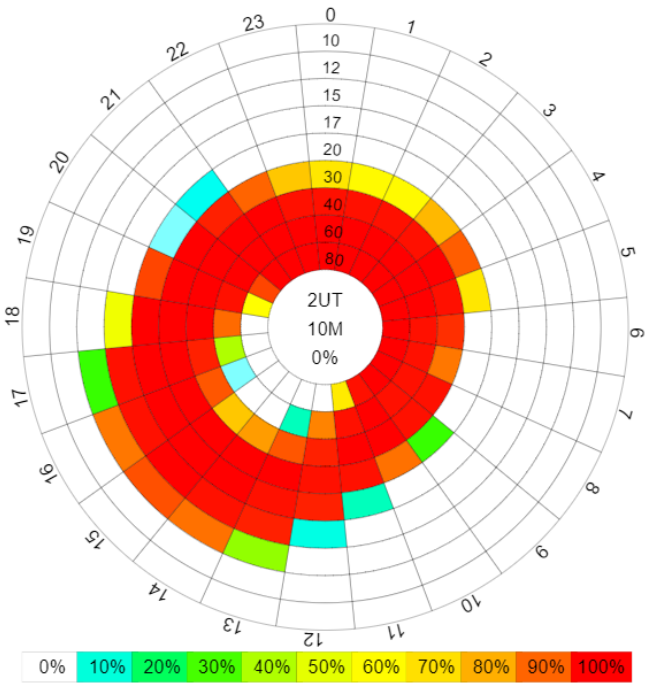


Figure 5.4: 24-hour propagation prediction wheel (Source: [40])

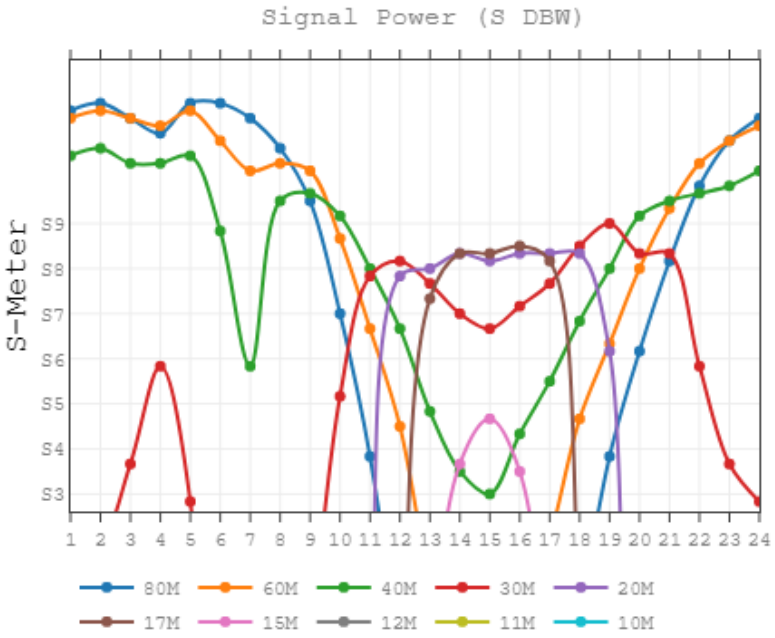


Figure 5.5: SDBW chart (Source: [40])

# CHAPTER 6. SIMULATION RESULTS

We are going to simulate the link every month of the 2020 year. As the performance of the communication depends on the state of the ionosphere, the results will be analysed season by season. In all cases, the transmitting power will be 160 W (the 80% of the value introduced in VOACAP, 200 W) unless the system requires an increase.

Although VOACAP simulates the performance of the communication working on all amateur bands, we are going to focus on the most relevant ones, that are from 40 meter to 15 meter. 80 meter and 60 meter amateur bands are not analysed as the chosen antenna cannot provide communication on this frequencies, and bands below 15 meter are not reliable in this case.

Also, all simulations are done assuming a 1F2 propagation mode. This means that the radio waves will be reflected two times by the F2-layer before reaching the receiver, as explained in 2.4..

Finally, remember to consider that we have to add one hour to the ones shown in the charts as the receiver is located in the United Kingdom (UTC+1).

## 6.1. Winter Season

We start simulating the performance of the link for the winter months. For this season we will select three different amateur bands: 40 meter, 30 meter and 20 meter bands.

This decision can be explained looking at Figure 6.1. As it can be seen, with a transmitting power of 160 W, the 40M band has a reliability above 95% practically all the day during December and January. On the contrary, in February at daytime, as the ionisation increases, this value decreases due to the absorption of the D-layer. As explained in Chapter 1, the absorption of the D-layer is only significant below 10 MHz and during the day, so in our link it only affects the 40M band when the solar rays ionise the ionosphere.

If we only look at the reliability charts, we could think that for example in January we can operate always on the 40 meter band. Although it is a very reliable band, it is interesting to look at the SDBW charts before making any decision. In Figure 6.2 it can be seen how there are bands that offer higher power levels than the 40 meter band, so it could be a good idea to change the operation frequency a few hours.

It is also remarkable the fact that as we are getting closer to March's equinox, the performance of the 15 meter band becomes better. This happens because it is very variable and depends a lot on solar activity and, as explained in Chapter 1, the spring equinox happens in March and this increases the ionisation of the ionosphere.

In conclusion, the selected bands for the winter season are specified in Table 6.1.

## 6.2. Spring Season

The second season we are going to analyse is spring, which goes from March to May. In this case, the selected bands will be also 40M, 30M and 20M.

A transmission power of 160 watts is still sufficient to reach 95% reliability, as it can be

seen in Figure 6.3. Furthermore, it is interesting to see how the 40 meter band continues to lose reliability at daylight hours. On the contrary, 30 meter and 20 meter amateur bands increase their reliability during the daytime as summer approaches.

Also, it can be seen how 15 meter band's reliability is greater in March than in April, as the equinox has already happened.

Furthermore, in Figure 6.3 (c) we can see the propagation prediction wheel for the month of May, where it can be verified that the most reliable bands is the 30 meter band, as it offers a high reliability during the whole day.

On the other hand, if we compare Figure 6.4 with Figure 6.2, we can see how the power levels have decreased, especially during the day. This happens because the absorption of the D-layer increases as summer approaches. At night, as this layer disappears, the power level does not change between seasons.

It is important to remember that we are simulating the link using a TX power of 160 W, but we can increase this value up to 2000 W if necessary and easily increase the received power.

Finally, the selected bands for the spring months are specified in Table 6.1.

## 6.3. Summer season

Now it is the turn of the summer season. Again, the selected bands will be 40M, 30M and 20M, as shown in Table 6.1.

As said before, the reliability of the 40 meter band during the night does not change as the D-layer disappears (see Figure 6.5). Even so, as in summer there are more hours of daylight, the 40 meter band becomes totally unusable during the day.

On the other hand, the 15 meter band becomes unusable, probably as a consequence of the low sunspot number for this months. Also, the 17 meter band becomes very variable and so it is best not to use this band as its performance would be unpredictable.

With respect to the SDBW charts, they are not relevant as they are practically identical to the one of May.

## 6.4. Autumn season

Finally, we will analyse the performance of the link in autumn. In Figure 6.6 it can be seen how the performance of the different amateur bands start to look like the one in winter and the 40 meter band recovers its high reliability. If we take a look at the September chart, we can see a strange behaviour at 14:00 and 16:00 UTC: the reliability decreases from over 90% to 70%. Fortunately, there is a tool in VOACAP that can explain us what is happening.

The explanation is simple: the most reliable mode at these hours is not the same as in all the other simulations. Instead of doing two hops, at 14:00 UTC the radio waves will do 3 hops before reaching the receiver. Obviously, this means more attenuation for our signal and therefore a lower reliability. On the other hand, at 16:00 UTC, the signal will

be reflected by the F1-layer instead of the F2-layer. Here the signal has to be send with a lower takeoff angle and so it is more attenuated as it travels more time through the D-layer.

In regard to reliability, this is not really a problem, as we can use another amateur band at these hours, such as the 17 meter band. Even so, if we look at Figure 6.7 (a), we can see how in September the power levels are really low. In this case, we can increase the transmitting power to improve the performance. In Figure 6.7 (b) shows what happens if we set a TX power of 1500 W in VOACAP.

Taking into account the reliability improvement, in this particular month we are going to raise the TX power to 1500 W and avoid the 20 meter band.

On the other hand, it is also remarkable that in September takes place the other equinox of the year and its effects can be seen also in Figure 6.6 (a). In this chart it is shown how the 15 meter band significantly increases its reliability in relation to August (as it happens with March equinox).

To conclude this section, the selected bands for every month are specified in Table 6.1, as well as the hours when it is indicated to work with and the received power values.

## 6.5. Summary of the simulation results

Finally, to conclude this Chapter, the conclusions drawn from these simulations are going to be summarized. In this case, instead of organising the information by seasons, we will explain concisely when we should use each of the mentioned amateur bands.

**40 meter band**

- Except in summer, this band will be used mostly at night, from sunset to solar maximum at midday.
- In summer, it will be used at solar minimum, from midnight to sunrise

**30 meter band**

- This band will be used in transitions between 40 and 20 meter bands (or the 17 one in November). This transitions usually coincide with the hours when the solar maximum is approaching and the 40 meter band loses reliability.

**20 meter band**

- This band will be used during the solar maximum. In winter, this period of time is shorter. As we approach summer, the solar maximum lasts longer.

**17 meter band**

- This band will be only used in November, when the 20 meter band has an unusual behaviour. The performance of this band is practically the same as the one of the 20 meter band.

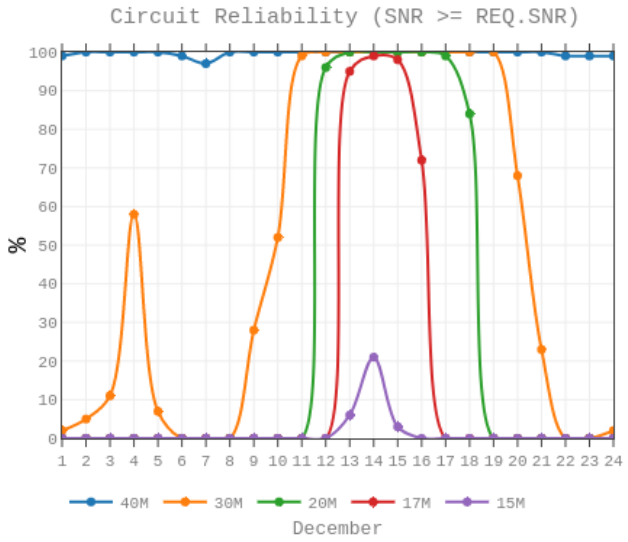


(a)

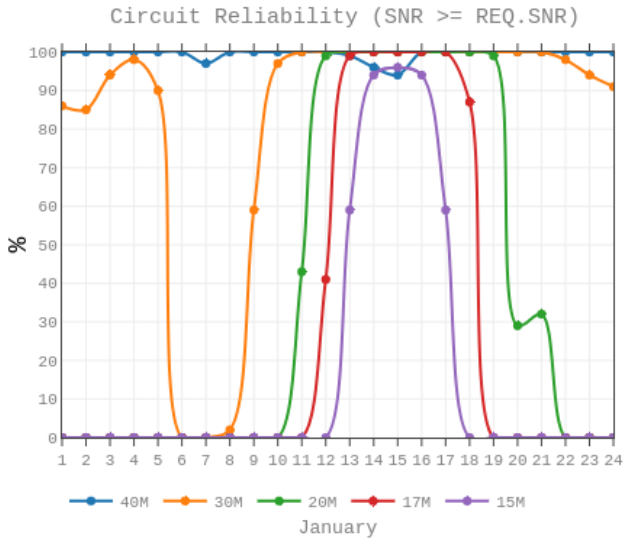


(b)

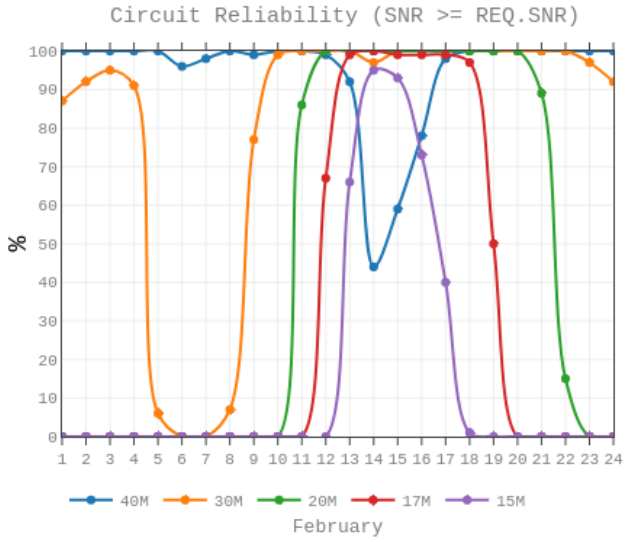


(c)

Figure 6.1: VOACAP reliability charts for December, January and February

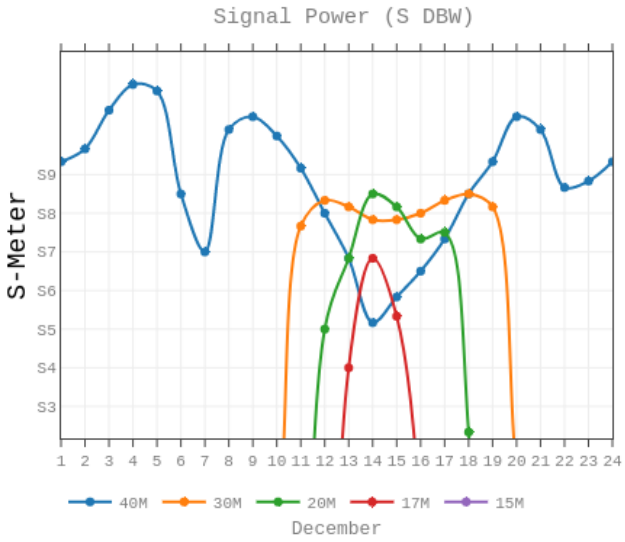


(a)

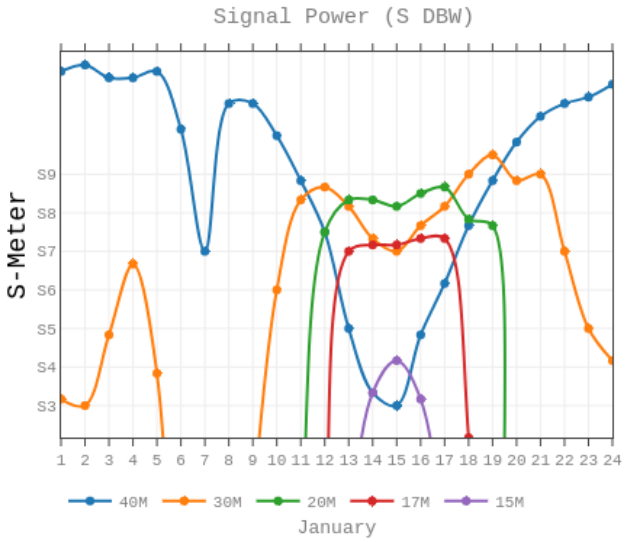


(b)

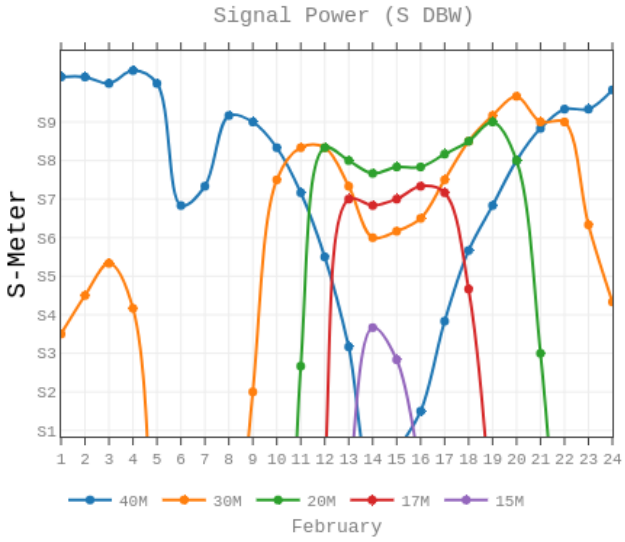


(c)

Figure 6.2: VOACAP SDBW charts for December, January and February

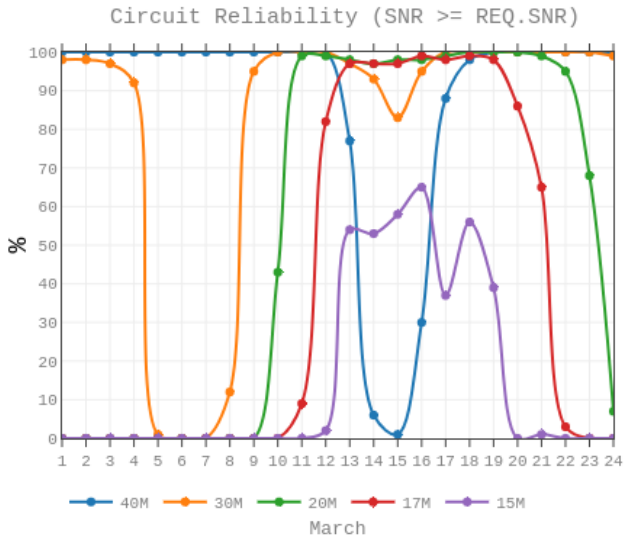


(a)

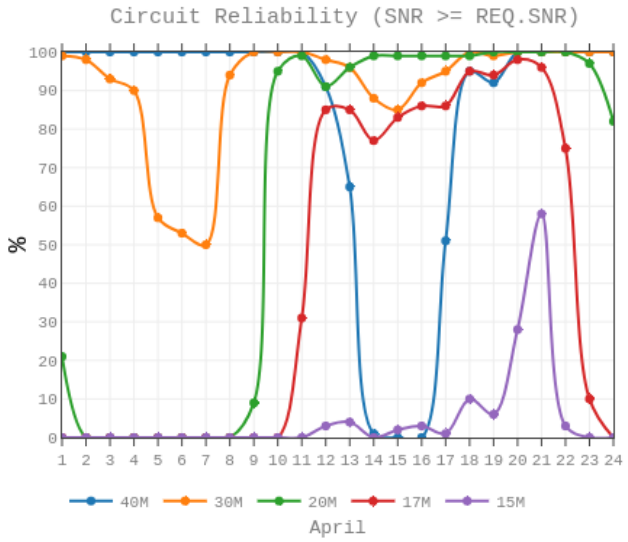


(b)

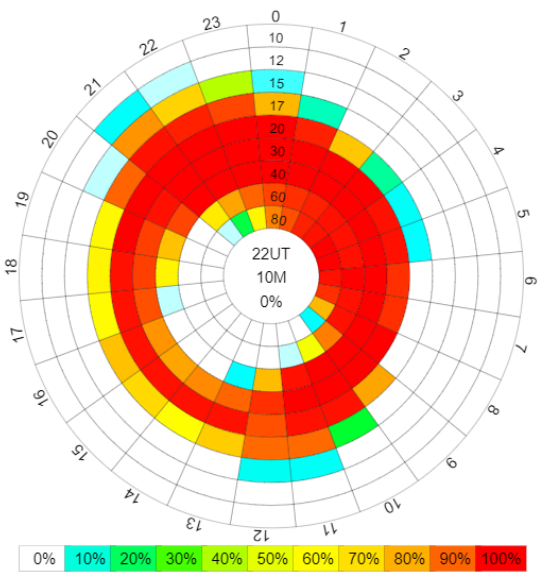


(c)

Figure 6.3: VOACAP reliability charts for March and April and Propagation Prediction Wheel for May

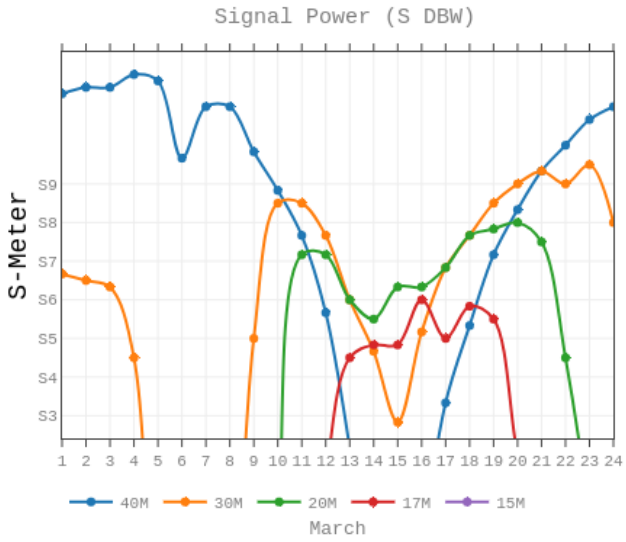


(a)

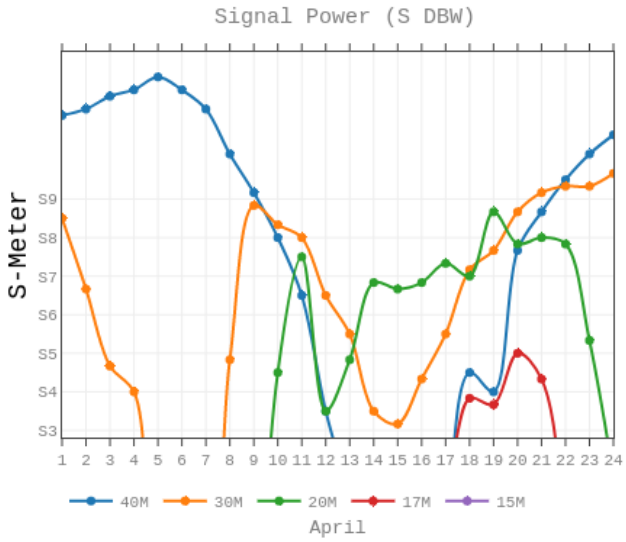


(b)

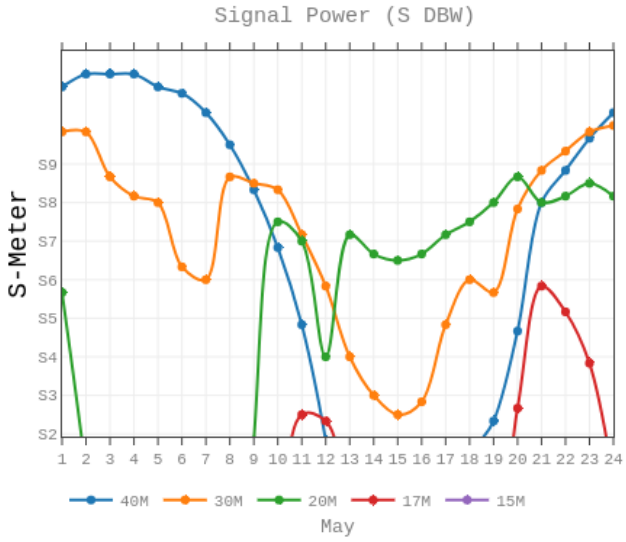


(c)

Figure 6.4: VOACAP SDBW charts for March, April and May

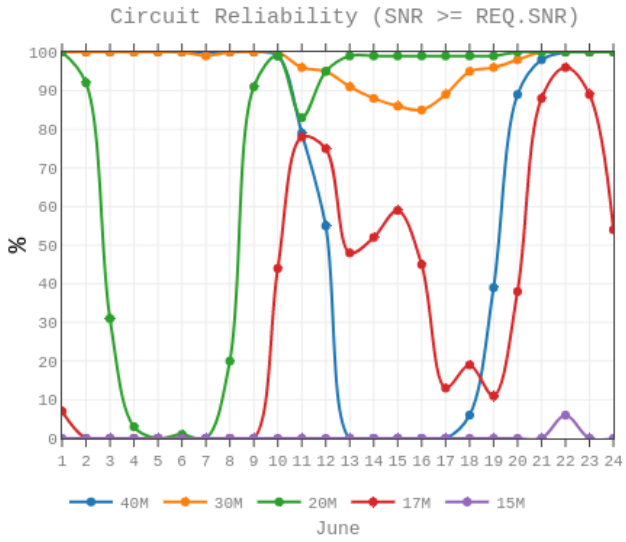


(a)

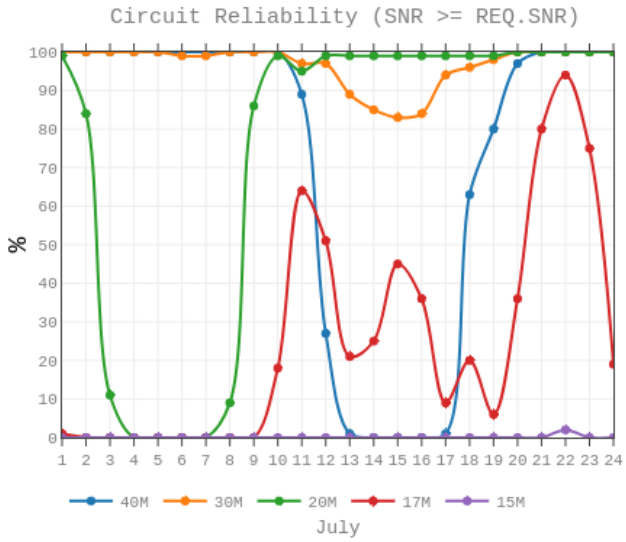


(b)

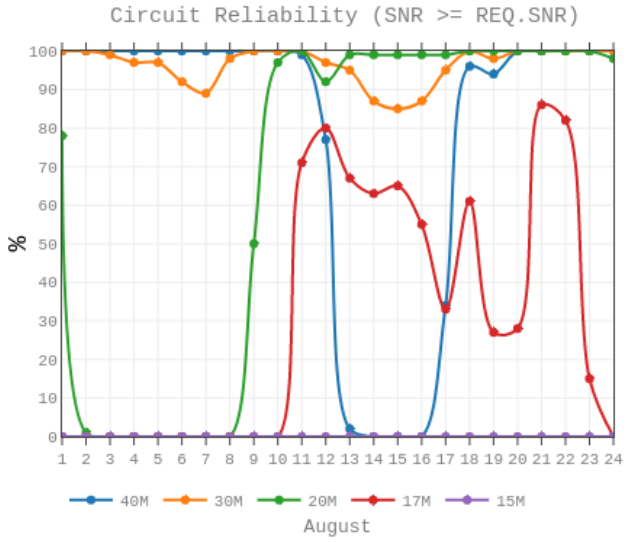


(c)

Figure 6.5: VOACAP reliability charts for June, July and August

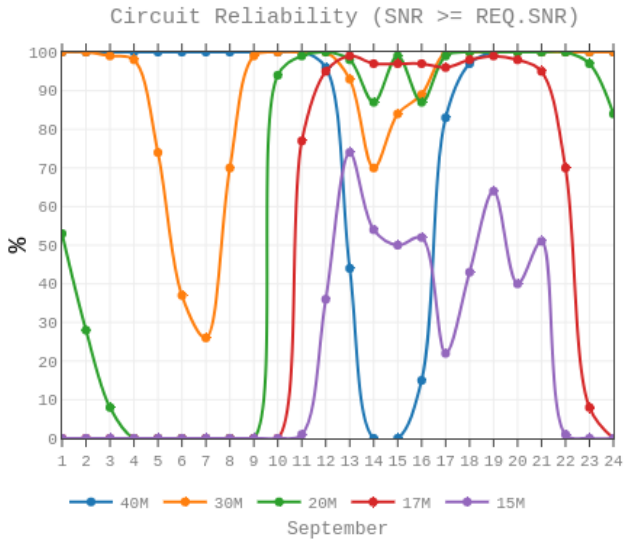


(a)

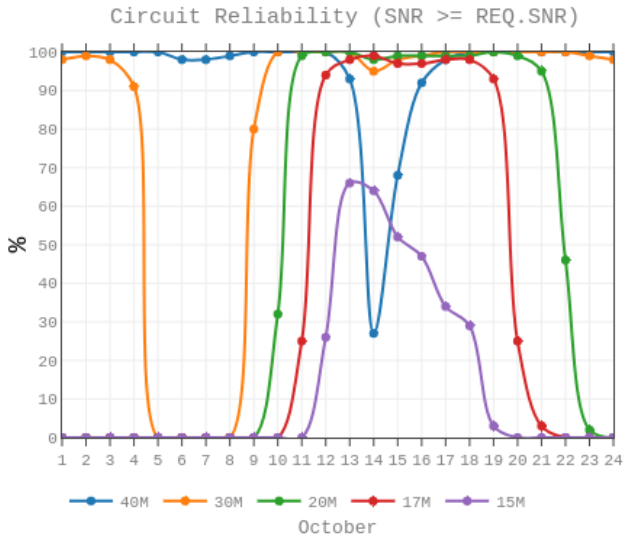


(b)

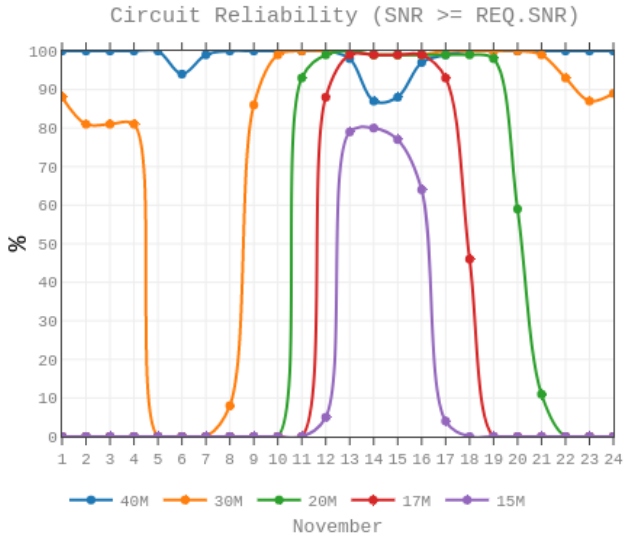


(c)

Figure 6.6: VOACAP reliability charts for September, October and November

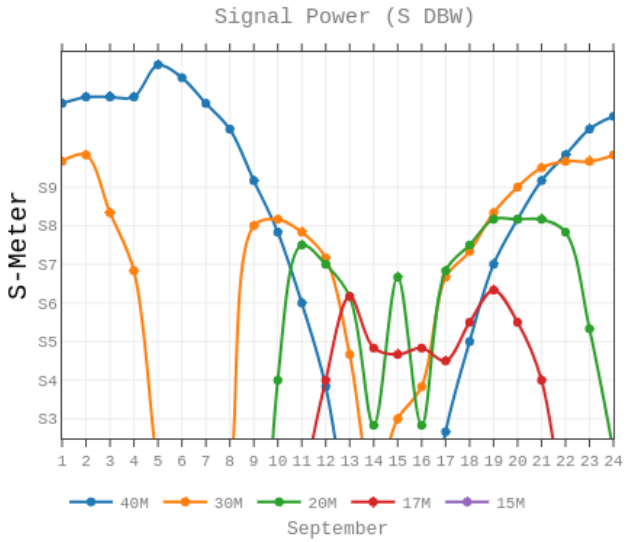


(a)

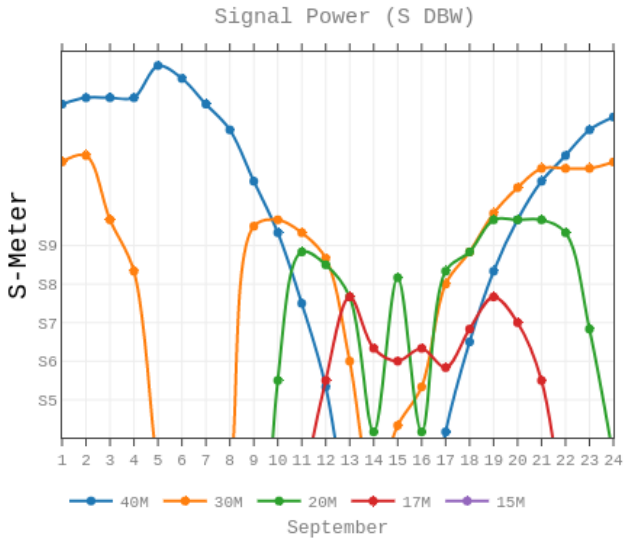


(b)

Figure 6.7: VOACAP SDBW charts for September with TX powers of 200 W and 1500 W

| Month | Hours of the day | Amateur Band | Power |
|---|---|---|---|
| December | 01-12 and 19-24 | 40M | S9 |
| | 12-14 and 16-19 | 30M | S9 |
| | 14-16 | 20M | S9 |
| January | 01-12 and 20-24 | 40M | S9 |
| | 12-13 and 18-20 | 30M | S9 |
| | 13-18 | 20M | S9 |
| February | 01-11 and 20-24 | 40M | S9 |
| | 11-12 and 18-20 | 30M | S9 |
| | 12-18 | 20M | S8-S9 |
| March | 01-11 and 22-24 | 40M | S9 |
| | 11-13 and 19-22 | 30M | S8-S9 |
| | 13-19 | 20M | S6-S8 |
| April | 01-10 and 22-24 | 40M | S9 |
| | 10-14 and 20-22 | 30M | S6-S9 |
| | 14-20 | 20M | S7-S9 |
| May | 01-09 | 40M | S9 |
| | 09-13 and 21-24 | 30M | S6-S9 |
| | 13-21 | 20M | S7-S9 |
| June | 01-08 | 40M | S9 |
| | 08-13 and 22-24 | 30M | S6-S9 |
| | 13-22 | 20M | S7-S9 |
| July | 01-08 | 40M | S9 |
| | 08-12 and 22-24 | 30M | S6-S9 |
| | 12-22 | 20M | S7-S9 |
| August | 01-09 | 40M | S9 |
| | 09-13 and 21-24 | 30M | S6-S9 |
| | 13-21 | 20M | S7-S9 |
| September | 01-10 and 22-24 | 40M | S9 |
| | 10-13 and 17-22 | 30M | S8-S9 |
| | 13-17 | 17M | S7-S8 |
| October | 01-11 and 21-24 | 40M | S9 |
| | 11-13 and 16-21 | 30M | S8-S9 |
| | 13-16 | 20M | S7-S8 |
| November | 01-12 and 20-24 | 40M | S9 |
| | 12-20 | 30M | S7-S9 |

Table 6.1: Selected amateur bands for different months

# CHAPTER 7. LATENCY COMPARISON BETWEEN HF AND OPTICAL FIBER LINKS

## 7.1. HF link

To compare the latency between optical fiber and HF links, the first thing we have to know is the distance that radio waves travel through the air.

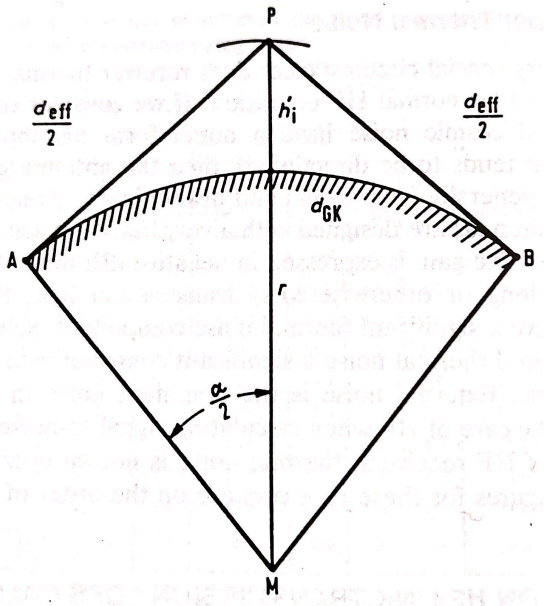


Figure 7.1: Geometric representation of a HF path between points A and B (Source: [3])

In Figure 7.1 some variables are defined. $A$ and $B$ are the transmitter and the receiver locations, $P$ the point of the ionosphere where the reflection occurs at $h'_i$ above the Earth's surface, and $d_{eff}$ the distance between points A, P and B. Also, $r$ is the radius of the Earth (6370 km) and $\alpha$ the great circle arc between A and B.

In our case, as explained in Section 4.6., the desired path will have two hops, so we must calculate the $d_{eff}$ two times: one between A and the midpoint of the path and one between it and B. Fortunately, we can assume that both hops are practically identical.

We are going to define $M$ as the midpoint between A and B at the coordinates 51° 10' 48.72" N 42° 4' 13.439" E (obtained from VOACAP, see Figure 7.3) and $P1$ and $P2$ as the two points of the ionosphere where the signal is reflected, as shown in Figure 7.2.

So, first of all, we calculate $\alpha$ from the great circle equation:

$$cos\alpha = \sin A \sin M + \cos A \cos M \cos \triangle L \tag{7.1}$$

where:

$A$ = latitude of the transmitter
$M$ = latitude of the midpoint
$\triangle L$ = longitude difference between $A$ and $M$

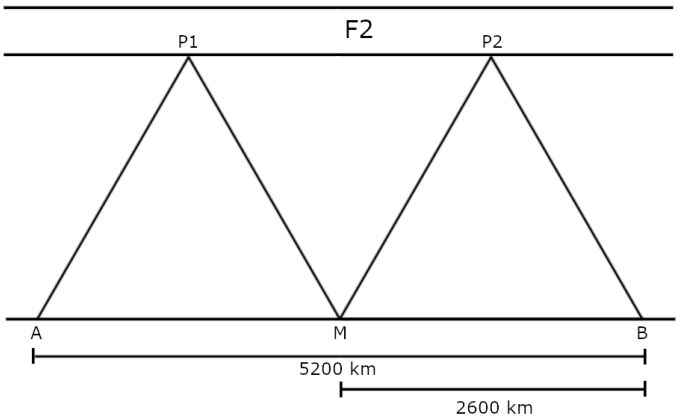


Figure 7.2: Schematic view of the path


Figure 7.3: VOACAP screenshot of the path's midpoint (Source: [40])

So, taking values defined in Section 4.2. we can calculate $\alpha$ [3]:

$$\alpha = 23.36^{\circ} \tag{7.2}$$

It is interesting to consider that the total great circle arc, that is the 46.72 $^{\circ}$ (twice the calculated value), represents almost a 13% of the total circumference of the Earth.

Once we have calculated $\alpha$, $d_{eff}$ can be calculated with Equation 7.3 [3]. To do this we need to define $h_i'$. As explained in Section 4.6., the height where the reflection will occur is around 300 km (with a takeoff angle of less than 10 degrees).

$$d_{eff} = 2\sqrt{8.115 \cdot 10^7 + 2rh_i' + h_i' - \cos\frac{\alpha}{2} \cdot (8.115 \cdot 10^7 + 2rh_i')} \tag{7.3}$$

$$d_{eff} = 2719.98km \tag{7.4}$$

So this is the distance of the path A-P1-M. To know the total distance (that is A-P1-M-P2-B) we just have to double the result:

$$d_{effT} = 2 \cdot 2719.98 = 5439.96km \tag{7.5}$$

Now, to calculate the latency of the link we have to know how fast radio waves propagate through the air. In Section 3.2. it has been determined that $v_{air}$ can be approximated to $3 \cdot 10^8 m/s$, so the latency of the HF link is:

$$5439.96 \cdot 10^3 m \cdot \frac{1}{3 \cdot 10^8}\frac{s}{m} = 18.1332 \cdot 10^{-3} s = 18.1332ms \tag{7.6}$$

## 7.2. Optical fiber link

Once we know the latency of the HF link, it is the turn of optical fiber.

In any optical fiber connection, we can consider three different latency contributions (see Figure 7.4):

- Serialization / Deserialization
- Optical-Electrical / Electrical-Optical conversion
- Optical Fiber

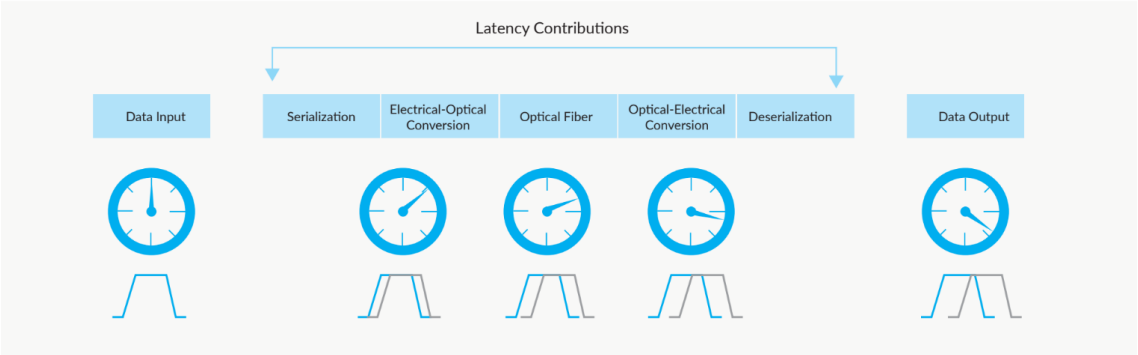


Figure 7.4: Latency contributions in an optical fiber system (Source: [43])

Serialization is a process in which blocks of data bits are broken into individual bits to facilitate its transportation. On the other hand, deserialization is the reverse process. The second contribution is the Electrical-Optical conversion. To transmit information, the electrical current must be converted to optical pulses of light. In reception we must do the reverse process. The last one is referred to the refraction index of the optical fiber and it is the main source of latency of the system. Due to this, we will not consider the two first latency contributions.

Currently, the most common connections between Europe and the United States are through submarine optical fibers. All these cables can be seen in a website called ”Submarine Cable Map” [44], as shows Figure 7.5.

Currently, there are over 1.2 million kilometres distributed between 378 submarine cables around the world. Sometimes they cover short distances, like the cable that connects the United Kingdom and Ireland, but they can also cover very long distances. In fact, the longest cable measures 20000 kilometres and allows communications between Asia and the United States [45].

These optical fibers lay on the bottom of the ocean floor and follow safe paths avoiding fishing and anchoring areas. Its installation is difficult and expensive as the ocean floor is not uniform and has hills and valleys. That is why before laying the cable an exhaustive study is done not only to know the variations of the bottom of the ocean but also to know its chemical composition or the temperature of the water (and detect possible volcanic activity) [46].

To be able to compare the latency of the HF and the fiber optic links, we have to look for a cable with a similar path. We have found two different cables that meet this condition.

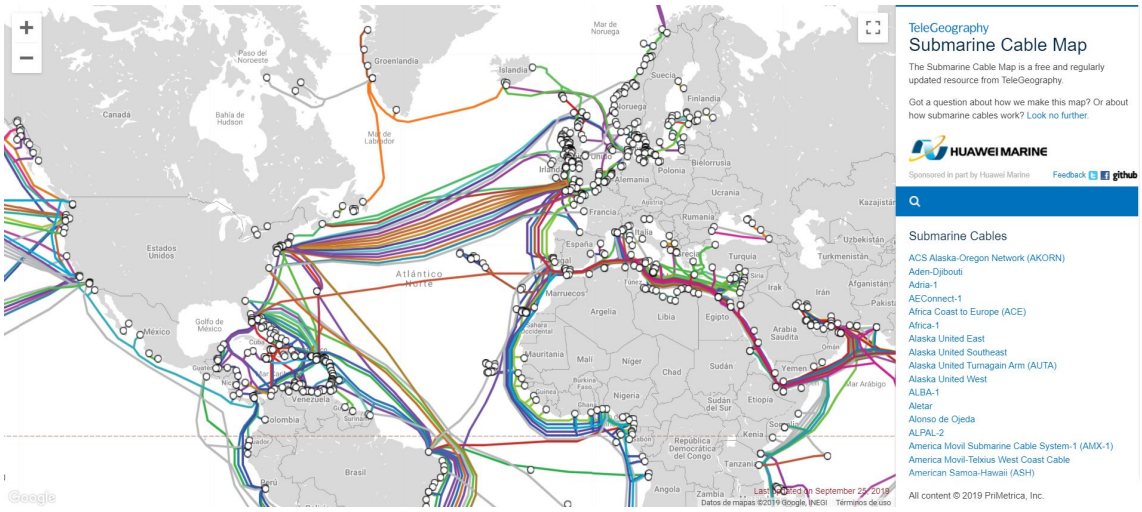


Figure 7.5: Submarine Cable Map website screenshot (Source: [44])

### 7.2.1. Apollo North cable

The first one is the Apollo North cable, that has a length of about 6500 kilometres. In Figure 7.6 two cables can be seen: Apollo North and Apollo South.

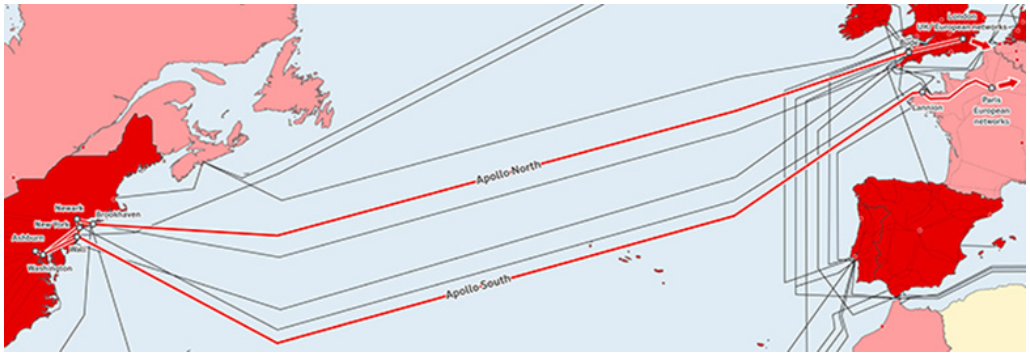


Figure 7.6: Apollo submarine cables (Source: [47])

We are going to focus on the first one, which connects Bude, in the United Kingdom, with Shirley, in New York, United States. Its owner is Vodafone, which guarantees a latency of 34.95 ms between the two ends of the link [47]. This value almost doubles the latency of the HF link.

To make sure that the given latency value is correct, we calculate the theoretical value.

As it has been explained in Section 3.2., it can be considered that the light travels through optical fiber at 2/3 of the speed through the air, as it has been calculated in Chapter 3.

$$6500 \cdot 10^3 m \cdot \frac{1}{2/3 \cdot 3 \cdot 10^8} \frac{s}{m} = 32.5 \cdot 10^{-3} s = 32.5 ms \tag{7.7}$$

As it was expected, both values are similar.

### 7.2.2. Yellow/AC-2 cable

The second one is the Yellow or AC-2 cable. It has a length of 6200 kilometres and links Bude and Bellport, in New York, and its owner is Century Link. In Figure 7.7 there are different submarine cables, among which is the one we are focusing on.

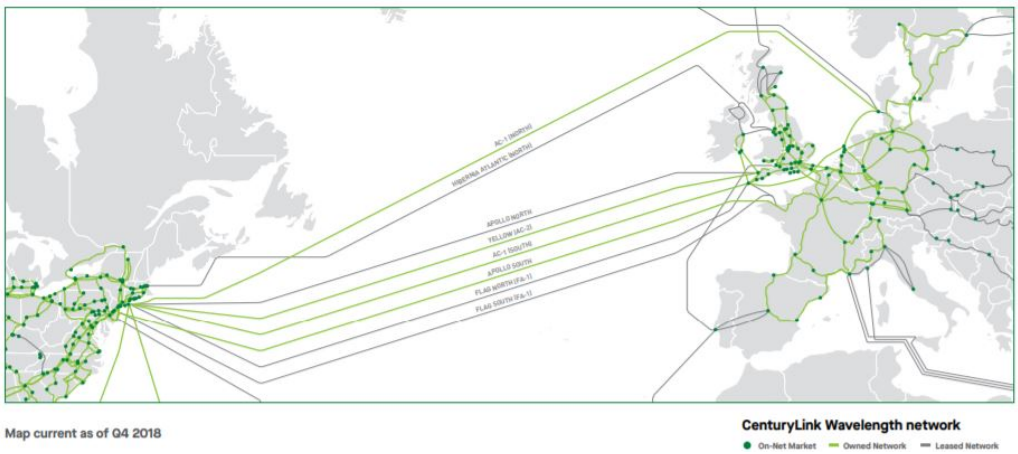


Figure 7.7: Yellow/AC-2 submarine cable (Source: [48])

We do not have data about its latency, so we are going to calculate the theoretical value:

$$6200 \cdot 10^3 m \cdot \frac{1}{2/3 \cdot 3 \cdot 10^8} \frac{s}{m} = 31 \cdot 10^{-3} s = 31 ms \tag{7.8}$$

In this case, although the value is lower than in the first submarine cable, the latency of the HF link is still the lowest.

# CONCLUSIONS

This project has been carried out with the aim of demonstrating that it is possible to establish a transoceanic shortwave radio link with a lower latency than the optical fiber one. At this point, the present study has proved that the latency of the HF link is by far lower than the one of the optical fiber. Specifically, the difference between the two values is about 13 milliseconds, so enterprises may take advantage of this.

In addition, we have met other of the basic requirements of the communication: reach a high reliability value. As it was proposed before simulating the link, we can guarantee a reliability above 95% throughout the year. This means that the communication can fail less than a day per month, although it is true that we have renounced to transmit huge amounts of information to reduce the intersymbol interference. In addition, it is also important to remember that all simulations have been done with low transmitting power values. This works in our favour, as we can increase the power to achieve better reliability levels.

Nevertheless, a distinction should be made between the different seasons of the year. Winter is the better season to use this link and summer the worst. In all of them, the amateur bands chosen to operate are the same: 40M at night, 30M at transition hours and 20M (or exceptionally 17M) during solar maximum.

However, there is no doubt that optical fiber is by far more reliable, as it does not depend on the behaviour of the ionosphere, and it also provides much more bandwidth. Even so, it is also remarkable that the deployment and maintenance of submarine optical fibers is very expensive compared with the shortwave link.

In view of these considerations, we can conclude that a HF link can never substitute an optical fiber one, but it can help in certain cases. For example, if we want to transmit little data with a low latency, we can use the HF link (providing the ionosphere allows it). So, a good option could be to combine both links and use the radio link only when needed.

# BIBLIOGRAPHY


[1] Schneider, D. (2018, June 1). Wall Street Tries Shortwave Radio to Make High-Frequency Trades Across the Atlantic. Retrieved October 13, 2019, from https://spectrum.ieee.org/tech-talk/telecom/wireless/wall-street-tries-shortwave-radio-to-make-highfrequency-trades_across-the-atlantic 3, 26

[2] ITU-R. (2015). *Nomenclature of the frequency and wavelength bands used in telecommunications* (Recommendation ITU-R V.431-8). Retrieved from https://www.itu.int/dms_pubrec/itu-r/rec/v/R-REC-V.431-8-201508-I!!PDF-E.pdf 5

[3] Freeman, R. L. (1991). *Telecommunication Transmission Handbook* (3rd ed.). New York, U.S.: Wiley. xiii, xiv, xv, 5, 9, 10, 11, 15, 16, 18, 19, 20, 21, 55, 56

[4] ITU-R. (1998). *Handbook, the Ionosphere and Its Effects on Radiowave Propagation: A Guide with Background to ITU-R Procedures for Radioplanners and Users*. Retrieved from https://www.itu.int/dms_pub/itu-r/opb/hdb/R-HDB-32-1998-PDF-E.pdf xv, 5, 6, 21

[5] Direccion General de Protección Civil y Emergencias. Gobierno de España. (2017, June). Red Radio de Emergencia - REMER. Dirección General de Protección Civil y Emergencias - Ministerio del Interior - España. VADEMECUM REMER. Retrieved October 12, 2019, from http://www.proteccioncivil.es/catalogo/carpeta02/carpeta24/vademecum17/vade01.htm xiii, 5, 6, 7, 8, 9, 14, 15, 16, 17

[6] Australian Government. (2016). *Introduction to HF Radio Propagation*. Retrieved from http://www.sws.bom.gov.au/Category/Educational/Other%20Topics/Radio%20Communication/Intro%20to%20HF%20Radio.pdf xiii, 5, 9, 11, 17, 18, 19, 21

[7] Eaves, J., & Reedy, E. (2012). *Principles of Modern Radar*. Retrieved from https://books.google.es/books?id=NHXjBwAAQBAJ&printsec=frontcover&hl=es&source=gbs_ge_summary_r&cad=0#v=onepage&q&f=false xv, 6

[8] Pritchard, J. (1989). *Newnes Short Wave Listening Handbook*. Retrieved from https://books.google.es/books?id=N4jgBAAAQBAJ&printsec=frontcover&hl=es&source=gbs_ge_summary_r&cad=0#v=onepage&q&f=false 8

[9] Poole, I. (November 1998). *Radio Waves and the Ionosphere*. Retrieved from https://www.arrl.org/files/file/Technology/pdf/119962.pdf 8

[10] Yadav, M. K., & Greeta, R. (2014). The ionosphere and radio propagation. *INTERNATIONAL JOURNAL OF ELECTRONICCOMMUNICATION ENGINEERING & TECHNOLOGY (IJECET)* , 5(11), 09–16. Retrieved from https://pdfs.semanticscholar.org/f719/f7c8aa369c333b4b2a7e5d72915f0ad6b93e.pdf 9

[11] EESA. (n.d.). TEC-EPS - Daily Sun Spot Number. Retrieved October 13, 2019, from http://space-env.esa.int/index.php/Daily-Sun-Spot-Number.html 10

[12] National Aeronautics and Space Administration (NASA). (2014, October 23). Largest Sunspot of Solar Cycle. Retrieved October 13, 2019, from https://www.nasa.gov/content/goddard/largest-sunspot-of-solar-cycle xiii, 10

[13] ITU. (n.d.). Frequency Bands allocated to Terrestrial Broadcasting Services. Retrieved October 13, 2019, from https://www.itu.int/en/ITU-R/terrestrial/broadcast/Pages/Bands.aspx xiii, 13

[14] RSGB. (n.d.). HF bands - Radio Society of Great Britain - Main Site : Radio Society of Great Britain – Main Site. Retrieved October 13, 2019, from https://rsgb.org/main/operating/band-plans/hf/ 13, 14, 15

[15] IARU. (2009, March 15). HF - International Amateur Radio Union - Region 1. Retrieved October 13, 2019, from https://iaru-r1.org/index.php/spectrum-and-band-plans/hf 13, 14, 15

[16] IARU. (2016, October 14). Plan de bandas - International Amateur Radio Union – Región 2: Region 2. Retrieved October 13, 2019, from https://www.iaru-r2.org/plan-de-bandas/ xv, 14

[17] ITU-R. (2019). *Radio Noise*. Retrieved from https://www.itu.int/dms_pubrec/itu-r/rec/p/R-REC-P.372-14-201908-I!!PDF-E.pdf xiii, 20, 21, 22

[18] CFTC Technical Advisory Committee (Ed.). (n.d.). *Sub-Committee on Automated and High Frequency Trading – Working Group 1*. Retrieved from https://www.cftc.gov/sites/default/files/idc/groups/public/@newsroom/documents/file/wg1presentation062012.pdf 23

[19] Duhigg, C. (2014, November 10). Stock Traders Find Speed Pays, in Milliseconds. Retrieved October 13, 2019, from https://www.nytimes.com/2009/07/24/business/24trading.html 23

[20] Rennison, J. (2018, January 1). How high-frequency trading hit a speed bump. Retrieved October 13, 2019, from https://www.ft.com/content/d81f96ea-d43c-11e7-a303-9060cb1e5f44 xiii, 23

[21] Segura, J. (2018, August 18). Qué es el High-Frequency Trading y por qué es peligroso. Retrieved October 13, 2019, from https://estrategafinanciero.com/que-es-el-high-frequency-trading-y-por-que-es-peligroso/ 23

[22] Nanex Research. (2012, August 9). Friends without Benefits. Retrieved October 13, 2019, from http://www.nanex.net/aqck2/3528.html xiii, 24

[23] Elliott, B., & Gilmore, M. (2002). *Fiber Optic Cabling*. Retrieved from https://www.academia.edu/34941907/Fibre_Optic_Cabling?auto=download 25

[24] Laumonier, A. (2018, July 13). Shortwave Trading — Part III — Fourth Chicago Site, East Coast, Patent, Regulation, and Farmer Kevin Mystery [Blog post]. Retrieved October 13, 2019, from https://sniperinmahwah.wordpress.com/2018/07/13/shortwave-trading-part-iii-fourth-chicago-site-east-coast-patent_regulation-and-farmer-kevin-mystery/ xiii, 26

[25] Goldin, A., Hutchins, J., & Malyshev, M. (2016). *Data Transmission via a High Frequency Radio Band* (United States Patent Application 20160173360). Retrieved from http://www.freepatentsonline.com/20160173360.pdf 30, 34

[26] Laumonier, A. (2018). SEE YOU IN A MONTH (OR 2592000000000 MICROSECONDS) [Blog post]. Retrieved October 13, 2019, from https://sniperinmahwah.wordpress.com/2018/ 28

[27] FCC Office of Engineering and Technology. (n.d.). APPLICATION FOR NEW OR MODIFIED RADIO STATION UNDER PART 5 OF FCC RULES - EXPERIMENTAL RADIO SERVICE (OTHER THAN BROADCAST). Retrieved October 13, 2019, from https://apps.fcc.gov/oetcf/els/reports/442_Print.cfm?mode=current 28

[28] Skycast Services. (n.d.). Who we are. Retrieved October 13, 2019, from http://skycastservices.com/ 28

[29] M2 Antenna Systems, Inc.. (2014). *10-30LP8 Manual.* Retrieved from https://www.m2inc.com/content/PDF%20MANUALS/LOGS%20HF/10-30LP8MAN02-W.pdf xv, 30, 31

[30] M2 Antenna Systems, Inc.. (2014b). *7&10-30LP8 Manual.* Retrieved from https://static.dxengineering.com/global/images/instructions/msq-71030lp8.pdf xv, 30, 31

[31] Balanis, C. A. (2005). *Antenna Theory: Analysis and Design* (3rd ed.). New Jersey, U.S.: John Wiley & Sons. xiii, 31

[32] Bevelacqua, P. (n.d.). VSWR. Retrieved October 13, 2019, from http://www.antenna-theory.com/definitions/vswr.php 32

[33] A. H. Systems. (n.d.). VSWR vs Return Loss Cheat Sheet. Retrieved October 13, 2019, from https://www.ahsystems.com/notes/VSWR-return-loss-sheet.php xv, 32

[34] Taylor, J. (2009). *WSPR 2.0 User's Guide*. Retrieved from https://www.physics.princeton.edu/pulsar/K1JT/WSPR_2.0_User.pdf xv, 33

[35] Taylor, J. (2019). *The FT4 Protocol for Digital Contesting*. Retrieved from https://physics.princeton.edu/pulsar/k1jt/FT4_Protocol.pdf xv, 33

[36] Hinson, G. (2018). *FT8 Operating Guide*. Retrieved from https://www.physics.princeton.edu/pulsar/K1JT/FT8_Operating_Tips.pdf xv, 33

[37] Silicon Labs. (2015, August 21). Knowledge Base. Retrieved October 13, 2019, from https://www.silabs.com/community/wireless/proprietary/knowledge-base.entry.html/2015/08/21/modulation/_choice-oUw0 xiii, 33

[38] Heise Online. (2018, April). Börsenhandel beschert Kurzwellenfunk ein Comeback. Retrieved October 13, 2019, from https://www.heise.de/newsticker/meldung/Boersenhandel-beschert-Kurzwellenfunk-ein-Comeback-4008891.html 34

[39] Perkiomaki, J. (n.d.). VOACAP Quick Guide: HF Propagation Prediction and Ionospheric Communications Analysis. Retrieved October 13, 2019, from https://www.voacap.com/ 35

[40] VOACAP. (n.d.). VOACAP Online HF Predictions. Retrieved October 13, 2019, from https://www.voacap.com/hf/ xiii, xiv, 35, 36, 37, 40, 41, 56

[41] OH6BG. (2018, June 17). VOACAP Online HF Predictions, User's Manual [Blog post]. Retrieved October 13, 2019, from https://voacap.blogspot.com/2018/06/voacap-online-hf-predictions-users.html xv, 35, 36, 38, 39, 40

[42] SILSO. (2019, October). Forecasts : McNish & Lincoln method. Retrieved October 14, 2019, from http://www.sidc.be/silso/prediml xiii, 38

[43] Commscope (s.f.). *Latency in optical fiber systems*. Retrieved from https://www.commscope.com/Docs/Latency_in_optical_fiber_systems_WP-111432-EN.pdf xiv, 57

[44] TeleGeography. (n.d.). Submarine Cable Map. Retrieved October 13, 2019, from https://www.submarinecablemap.com/ xiv, 57, 58

[45] TeleGeography. (n.d.). Submarine Cable FAQs. Retrieved October 13, 2019, from https://www2.telegeography.com/submarine-cable-faqs-frequently-asked-questions 57

[46] Techteledata. (n.d.). How submarine cables are made, laid, operated and repaired — TechTeleData - Broadband Infrastructure and Consultancy. Retrieved October 13, 2019, from https://web.archive.org/web/20160526231647/http://www.techteledata.com/how-submarine-cables-are-made-laid-operated-and-repaired/ 57

[47] Vodafone. (s.f.). Connectivity — Apollo Submarine Cable System. Retrieved 13 October, 2019, from https://www.vodafone.com/business/news-and-insights/blog/gigabit-thinking/apollo-submarine-cable-system xiv, 58

[48] Century Link. (n.d.). *Wavelength Transatlantic Service*. Retrieved from https://www.centurylink.com/asset/business/enterprise/network-map/en-br-wavelength-transatlantic-systems-br180019.pdf xiv, 59